Intrinsic Sources of Tachykinin-Related Peptide in the Thoracic Ganglion Mass of the Crab, *Cancer borealis*

Amanda N. Rainey
Stephanie M. Fukui
Katie Mark
Hailey M. King
Dawn M. Blitz[1]

Department of Biology and Center for Neuroscience
Miami University
Oxford OH 45056

[1]Corresponding Author:
Dawn M. Blitz
700 E High St
PSN 212
Oxford OH, 45056
blitzdm@miamoh.edu
513-529-6327

Neuropeptides comprise the largest class of neural and neuroendocrine signaling molecules. Vertebrate tachykinins (TKs) and the structurally-related invertebrate tachykinin-related peptides (TRPs) together form the largest neuropeptide superfamily, with a number of conserved neural and neuroendocrine functions across species. Arthropods, including crustaceans, have provided many insights into neuropeptide signaling and function. Crustacean tachykinin-related peptide occurs in endocrine organs and cells and in two of the major crustacean CNS components, the supraoesophageal ganglion (“brain”) and the stomatogastric nervous system. However, little is known about TRP sources in the remaining major CNS component, the thoracic ganglion mass (TGM). To gain further insight into the function of this peptide, we aimed to identify intrinsic TRP sources in the TGM of the Jonah crab, *Cancer borealis*. We first adapted a clearing protocol to improve TRP immunoreactivity specifically in the TGM, which is a dense, fused mass of multiple ganglia in short-bodied crustaceans such as *Cancer* species of crabs. We verified that the clearing protocol avoided distortion of cell body morphology yet increased visibility of TRP immunoreactivity. Using confocal microscopy, we found TRP-immunoreactive (TRP-IR) axon tracts running the length of the TGM, TRP-IR neuropil in all ganglia, and approximately 110 TRP-IR somata distributed throughout the TGM, within and between ganglia. These somata likely represent both neural and neuroendocrine sources of TRP. Thus, there are many potential intrinsic sources of TRP in the TGM that are positioned to regulate behaviors such as food intake, locomotion, respiration, and reproduction.

Keywords: neuropeptide, neuroendocrine, crustacean, immunohistochemistry, confocal

Abbreviations: ACO, anterior commissural organ; AG, abdominal ganglion; TRP, tachykinin-related peptide; TRP-IR, tachykinin-related peptide immunoreactive; TRP_{CT}, tachykinin-related peptide central tract; *coc*s, circumoesophageal connectives; CoGs, commissural ganglia, *poc:* postoesophageal commissure; SA, sternal artery; SoG, suboesophageal ganglion; STG, stomatogastric ganglion; T1-T5, thoracic ganglia 1-5; TGM, thoracic ganglion mass.

1. Introduction

Neuropeptides comprise the largest class of neural and neuroendocrine signaling molecules (Cropper et al., 2018; Jékely et al., 2018; Katz and Calin-Jageman, 2008; Nusbaum et al., 2017; Skiebe, 2001; Smith et al., 2019; Taghert and Nitabach, 2012). The form and function of many neuropeptides are highly conserved between vertebrates and invertebrates (Buma and Roubos, 1986; Chowanski et al., 2017; Kim et al., 2017; Nässel, 2006; Taghert and Nitabach, 2012). To mediate their effects, neuropeptides can be released at classical synapses or non-synaptic sites to reach nearby targets in a paracrine fashion, and hormonally to have wide-ranging effects (Buma and Roubos, 1986; Cropper et al., 2018; Jékely et al., 2018; Landgraf and Neumann, 2004). Although there is increasing information regarding neuropeptide functions, particularly in motor and sensory systems (Cropper et al., 2018; Jékely et al., 2018; Nässel et al., 2019; Nusbaum and Blitz, 2012; Taghert and Nitabach, 2012), there is much less known regarding the natural stimuli that activate peptidergic neurons and trigger neuropeptide release (Chowanski et al., 2017; Skiebe, 2001; Taghert and Nitabach, 2012). Anatomical analyses of peptidergic neurons can provide a framework for identifying inputs, and therefore physiological stimuli, that regulate peptidergic neuron activity.

Vertebrate tachykinins (TKs) comprise one of the largest known neuropeptide families and have a high degree of conservation with invertebrate analogs, the tachykinin-related peptides (TRPs) (Chowanski et al., 2017; Harrison and Geppetti, 2001; Nässel et al., 2019; Steinhoff et al., 2014; Taghert and Nitabach, 2012). Vertebrate TKs and invertebrate TRPs share a similar C terminal amino-acid sequence (Phe-x-Gly-Leu-Met-NH_2 vs Phe-x-Gly-y-Arg-NH_2) and bind to similar receptors (Nässel et al., 2019; Steinhoff et al., 2014). TKs and TRPs also regulate many of the same behaviors and functions in their respective organisms, including feeding, foraging, aggression, digestion, and reproduction (Chowanski et al., 2017; Doi and Ramirez, 2008; Harrison and Geppetti, 2001; Kim et al., 2017; Nässel et al., 2019; Steinhoff et al., 2014; Taghert and Nitabach, 2012; Winther et al., 2006). Both TKs and TRPs act as local and hormonal signaling molecules across organisms (Harrison and Geppetti, 2001; Nassel, 1999; Nässel, 2006; Nässel et al., 2019; Steinhoff et al., 2014; Winther et al., 2006). Due to the extent of conservation between TKs and TRPs, plus the smaller size and greater accessibility of invertebrate nervous systems, much can be learned about the function and regulation of this peptide superfamily using invertebrate organisms (Chowanski et al., 2017; Christie, 2011; Nässel et al., 2019).

Crustaceans have proven particularly useful in the study of neuropeptide signaling, from the early demonstration of neurosecretion, to numerous general principles of neuropeptide modulation of neural circuits, to comparative analyses of peptides and peptide families across species (Christie et al., 2010; Dickinson et al., 2016; Nusbaum et al., 2017). Immunocytochemistry, biochemistry, mass spectrometry, including mass spectral imaging, and genome/transcriptome mining have enabled the identification of many neuropeptides in crustacean neural and endocrine tissue (Chen et al., 2009a,b; Christie, 2011; Christie et al., 2015). However, the distribution of many of these peptides remains to be determined, particularly at the cellular level.

Neuroendocrine release in crustacea occurs from different types of structures including peripheral organs such as the X-organ-sinus gland complex in the eyestalk and the pericardial organ (PO) surrounding the heart, central organs such as the anterior commissural organ (ACO) located within the neuropil of a central ganglion, and additional neurosecretory terminals and cells distributed along nerves and the gut lining (Christie, 2011). TRP labeling occurs in most of these neuroendocrine sites, however, which combination of structures contains TRP varies across different crustacean species (Christie et al., 2010, 2007, 1995; Messinger et al., 2005). Here we focus on the Jonah crab, *Cancer borealis,* in which native TRP isoforms have been identified as *Cancer borealis* tachykinin-related peptide Ia and Ib (CabTRP Ia/Ib) (Christie et al., 1997). Both isoforms are recognized by the same antibody, but CabTRP Ia has higher bioactivity (Christie et al., 1997). In *C. borealis*, among endocrine structures, TRP immunoreactivity is present in the PO, ACO, and midgut epithelial cells (Blitz et al., 2008; Christie et al., 2007, 1995; Li et al., 2003; Swallie et al., 2015).

The major components of the crustacean CNS are the supraoesophageal ganglion ("brain"), the stomatogastric nervous system (STNS), and the ventral nerve cord, which is compressed into a fused thoracic ganglion mass (TGM) in short-bodied crabs such as *C. borealis* (Bullock and Horridge, 1965; Smarandache-Wellman, 2016). TRP immunoreactivity is present in neuropil and local interneuron somata in regions involved in processing olfactory, visual, and tactile information in the supraoesophageal ganglion (Chen et al., 2009a; Sandeman et al., 1990; Schmidt and Ache, 1994; Yasuda-Kamatani and Yasuda, 2006). However, most information about TRP function is regarding its actions within the STNS, a key system for studying neuromodulation at multiple levels of a motor system (Daur et al., 2016; Marder and Bucher, 2007; Stein, 2009).

The STNS controls feeding behaviors such as food chewing and filtering (Marder and Bucher, 2007). In particular, TRP is present in a modulatory projection neuron, intrinsic to the STNS, which modulates feeding motor circuits through paracrine actions (Blitz et al., 2008; Christie et al., 1997; Messinger et al., 2005; Stein et al., 2007; Swensen and Marder, 2000). TRP is also located in axon terminals forming a neuroendocrine organ, the ACO, within the STNS (Messinger et al., 2005). TRP release from the ACO triggers activation of a particular form of chewing through paracrine actions (Blitz et al., 2008; Diehl et al., 2013; White and Nusbaum, 2011). Additionally, hormonal TRP actions modulate muscles involved in chewing and food filtering behaviors (Messinger et al., 2005). The cells contributing to the ACO originate outside of the STNS and thus provide an extrinsic source of TRP to this area of the crustacean CNS. TRP is also present in the final crustacean CNS structure, the TGM (Blitz et al., 2008; Huybrechts et al., 2003; Schmidt, 1997), however, there is little information about its distribution within the TGM, with no information available for *C. borealis*.

In this study, we aimed to characterize TRP distribution in the TGM of *C. borealis*, with particular attention to sources that originate within the ganglion. We used immunofluorescence and confocal microscopy to visualize TRP-immunoreactive (TRP-IR) structures. Determining TRP distribution in the crab TGM is an important step toward identifying potential functional roles, which could extend to regulating behaviors such as ventilation, locomotion, food intake, and reproduction as is true for TKs and TRPs in other organisms (Doi and Ramirez, 2008; Harrison and Geppetti, 2001; Kahsai et al., 2010; Nassel, 1999; Steinhoff et al., 2014; Taghert and Nitabach, 2012; Winther et al., 2006).

2. Methods

2.1. Animals

C. borealis males (Fresh Lobster Company; Gloucester, MA) were housed in 10 °C recirculating salt water tanks. Crabs were anesthetized prior to dissection by packing them in ice (30-40 min). During dissection, the TGM was isolated from the cephalothorax then pinned in a Sylgard-lined Petri dish and maintained in chilled *C. borealis* saline (~ 4 °C). Under a dissecting microscope, the remaining fat and connective tissue were removed. The sternal artery was carefully trimmed close to the TGM in order to prevent damage to the tracts running near where the artery passes through the TGM.

2.2. Solutions

C. borealis saline (pH 7.4-7.6) was composed of: 440 mM NaCl, 26 mM $MgCl_2$, 13 mM $CaCl_2$, 11 mM KCl, 10 mM Trizma Base, and 5 mM Maleic Acid. Phosphate buffer (P) (pH 7.3) was a 2.3:1 ratio of sodium phosphate dibasic [1 M] and sodium phosphate monobasic [0.1 M]. P-Triton consisted of 3% Triton-X (Fisher Scientific) diluted in phosphate buffer.

2.3. Immunocytochemistry

Directly after dissection, TGMs were fixed in 4% paraformaldehyde in phosphate buffer solution for 12-24 hrs. After fixation, TGMs underwent five, 1 hr washes in P-Triton and were stored overnight (7-12 hr) in P-triton to permeabilize cell membranes before incubation with the primary antibody, rat anti-Substance P (monoclonal, generated against human Substance P; clone NC1/34, Accurate Chemical and Scientific Corporation catalog number YMC1021). The initial characterization of this antibody demonstrated that it binds to the C-terminal of Substance P, the conserved region across TK and TRPs, has low (5%) cross-reactivity with the TK, eledoisin, but no cross-reactivity with other peptides such as enkephalins, somatostatin, and β-endorphin (Cuello et al., 1979). Several lines of evidence support this antibody reacting with native TRPs in decapod crustaceans. First, in the crab nervous system, pre-adsorption of this antibody with CabTRP Ia blocks labeling (Christie et al., 1997; Christie et al., 2007).

Second, anti-Substance P labeling colocalizes with anti-locust TRP labeling in the STNS (Blitz et al., 1995). This includes a distinct neuroendocrine structure, also labeled by the Substance P antibody across many species (Messinger et al., 2005), and a pair of identified modulatory network inputs (Blitz et al., 1995; Blitz et al., 1999). Third, exogenous CabTRP Ia application mimics the actions of the anti-Substance P labeled neuroendocrine structure; a tachykinin receptor antagonist blocks the actions of the network inputs that label with the anti-Substance P antibody; and actions of both of these anti-Substance P labeled cell populations are prolonged by applying an inhibitor (phosphoramidon) of an extracellular endopeptidase that cleaves TKs (Wood et al., 2000; Blitz et al., 2008). Combined, these data support the conclusion that the anti-Substance P antibody used in this study labels native TRPs in *C. borealis*. Thus far, CabTRP isoforms are the only TRPs isolated from *C. borealis* neural and endocrine tissues using radioimmunoassay as well as multiple mass spectrometry techniques (Christie et al., 1997; Li et al., 2003; Chen et al., 2009a,b; Yu et al., 2014). However, because there may be additional, not yet identified TRP family members that cross-react with the Substance P antibody, we will refer to the Substance P antibody labeling as TRP immunoreactivity. Preparations were incubated with anti-Substance P (1:300) for 72 hrs on a shaker-plate at room temperature. Specimens then underwent an additional five, 1 hr washes with a final incubation of 7-12 hr in P-triton before incubation with the secondary antibody (goat anti-rat Alexa Fluor 488 or 563, 1:300; Invitrogen). Incubation with the secondary antibody occurred on a shaker plate at room temperature for 16-18 hr. Finally, the tissue underwent five, 1 hr rinses in phosphate buffer and were stored in phosphate buffer until mounting or clearing.

TGMs were mounted within a well consisting of either cover-slip stacks or a silicone gasket. Cover-slip stacks were created by sealing multiple coverslips together (2-5) with nail polish. Then one stack was placed along each side of a slide to create a rectangular well (Bucher, 2014; Swallie et al., 2015). Alternatively, silicone gaskets (Electron Microscopy Sciences) were glued onto slides using nail polish or Permount mounting medium (Fisher Scientific). Uncompressed or cleared specimens were mounted in wells that were five coverslips deep or made from 1 mm thick gaskets. Compressed specimens were mounted in chambers that were 2-3 coverslips deep or made from 0.5 mm gaskets. Uncleared specimens (both uncompressed and compressed), were mounted in glycerol solution (80% glycerol in 20% 20mM Na_2CO_3) or Vectashield (Vector Laboratories). Cleared TGMs were mounted in 100% methyl salicylate or Permount. Coverslips (#1.5) were used to cover the wells and sealed into place with nail polish or Permount.

2.4. Tissue Clearing

A clearing protocol was adapted for the TGM in *C. borealis* from previously reported procedures (Bucher, 2014; Kononenko et al., 2018; Nässel 1984; Richardson and Lichtman, 2015). Specifically, ultra-dry 200 proof Ethanol was prepared by pouring 200 proof anhydrous EtOH (Deacon Laboratories) over molecular sieves and allowing to dehydrate for 24 hours (Bucher, 2014; Thorn et al., 2007). The methyl salicylate used for rehydration was 100% reagent grade (Fisher Scientific) diluted with ultra-dry ethanol (EtOH). All solutions, with the exception of the ultra-dry EtOH, were made immediately prior to use to avoid water contamination.

Tissue was dehydrated through a graded series of EtOH concentrations diluted in reverse osmosis (RO) water; starting with incubation in 30% EtOH (1 hr), 50% (1 hr), 75% (1 hr), 95% (1 hr), and then incubated twice in 100% ultra-dry EtOH (1 hr each). Between each concentration, 3 quick (<1 sec) washes with the new solution were performed. After dehydration, TGMs were rehydrated in a desiccation chamber by incubating the preparation in 1:1 methyl salicylate/EtOH for 30 min, then in 3:1 methyl salicylate/ EtOH for 1 hr, and then in 100% reagent grade methyl salicylate in the desiccation chamber until mounting (15-60 min). Between each solution, specimens were rinsed 3 times (<1 sec) in the next solution.

2.5. Image Collection

Confocal micrographs were collected using the Zeiss 710 confocal microscope located in the Center for Advanced Microscopy and Imaging (CAMI; Miami University, Oxford OH). Images for this study were collected using 10x (EC Plan-Neofluar 10x/0.3 NA), 20x (Plan-apochromat 20x/0.8 NA), and 40x air (Neofluar 40x/0.75 NA) objectives. The 543 nm diode laser and Texas red filter set were used to collect images from preparations in which Alexa 568 was the fluorophore. The 488 nm Argon laser and the GFP filter set were used to collect images from preparations in which Alexa 488 was the fluorophore. Images were acquired with Zen Black software (Zeiss), which was also used to generate maximum intensity projections or 3D renderings from z-stacks of confocal images. In maximum intensity projections, z-stack optical sections are compressed into a single 2D plane. For each pixel location across the X-Y plane, the brightest intensity of that pixel from all optical sections in a z-stack is displayed. To produce a 3D image, pixels through a z-stack are used to build voxels which are then assembled into a rotatable image. In some figures, 2D images were generated after rotation of a 3D image as noted. In some images, a depth code, a color code that is based on the dorsal to ventral extent of each pixel, was applied to provide 3D information in a 2D image.

2.6. Data Analysis

TRP-IR cells were identified based on the presence of punctate staining and a non-immunoreactive nucleus. Cell size was determined using Zen Black software to measure the shortest (horizontal diameter) and longest (vertical diameter) distance through the center of the nucleus (Dircksen and Keller, 1988; Kornthong et al., 2014). For all identified cells, the horizontal diameters were used to assign cells to size classes based on previous classifications of crustacean neurons (Dircksen and Keller, 1988; Khornchatri et al., 2015; Kornthong et al., 2014; Yasuda et al., 2004). As a number of cell diameters were in gaps between the previously used size ranges, we expanded the ranges for cell size classes for this study. Specifically, the adjusted size classes (using horizontal diameters for classifications) were globuli, <9 µm; small, 9-16.9 µm; medium, 17-34.9 µm; large, 35-94.9 µm; giant, >95 µm.

Cells were counted in each ganglion through consecutive optical sections in a z-stack by using the drawing tool in Zen Black software to mark each cell with a circle then counting the circles. The ganglion in which each cell occurred was recorded along with diameter. The anterior-posterior and ventral-dorsal location of each cell was measured relative to a set of TRP-IR branches projecting from a dense TRP-IR axon bundle that projects centrally through the length of the TGM. This tract is referred to as the TRP central tract (TRP_{CT}) and is likely within the ring commissure, a bilateral longitudinal axon bundle that runs through the central-dorsal aspect of the TGM (Dircksen and Keller, 1988; Kornthong et al., 2014; Saetan et al., 2013). All cells were noted as ventral or dorsal based on whether they were ventral or dorsal to where the TRP_{CT} branches met the dorsal extent of the TRP_{CT} within a ganglion. The TRP_{CT} branches project near the anterior-posterior midline of each ganglion and were thus used to establish an anterior-posterior boundary for cells within each ganglion. Some TRP-IR cells were located in the spaces between each of the ganglia rather than within a ganglion. The depth of these inter-ganglionic cells was compared to the depth of the TRP_{CT} branch closest to the largest number of cells between each set of ganglia.

Axons were traced through a z-stack using the Bezier drawing tool in Zen Black software. First, the leading edge of the Bezier was placed on an axon exiting the soma. Then the Bezier line was continued by clicking on the axon as it was followed through the z-stack, scanning through z-planes. Most axon lengths spanned a greater x-y distance than could be obtained within a single z-stack. Thus, multiple z-stacks were obtained with overlap between the z-stacks. The location of an axon relative to a feature, such as distinctive neuropil or the sternal artery within the overlapped region, was noted in order to follow an axon from one z-stack to another.

2.7. Statistics

Statistical analysis was performed using Sigma Plot (Systat software) or Excel 2016 (Microsoft). Data are reported as mean ± SD. N values are reported as the number of animals (N) and/or the number of occurrences for structures that occur bilaterally (n). Fisher Exact Test was used to compare the number of tracts, cells, or other anatomical structures identified in compressed, uncompressed, and cleared TGMs. To correct for errors due to multiple (three) comparisons, the α value was adjusted to 0.017 using Bonferroni correction (McDonald, 2014). The number of visible cells across processing methods was compared using a One-Way ANOVA followed by a post hoc Holm-Sidak analysis. The horizontal and vertical diameters were compared between processing methods using One-Way ANOVA followed by a post hoc Holm-Sidak analysis.

2.8. Figures

All images and figures were assembled in Corel Draw (Corel Corporation, v16). Graphs were imported into Corel Draw from Sigma Plot (Systat software) or Excel 2016. Image collages were generated from consecutive, overlapping confocal micrographs. Maximum intensity projections of whole z-stacks or subsets were generated in Zen Black software and imported into Corel Draw. Once in Corel Draw, features shared between two micrographs were aligned using the transparency tool to verify overlap.

3. Results

3.1. Optimizing Visibility of TRP-IR Structures in the TGM

The TGM of short bodied crustaceans, such as *C. borealis*, consists of multiple ganglia fused into a ring around the sternal artery (SA) (Fig. 1A, B). The anterior-most ganglion in this fused mass is the suboesophageal ganglion (SoG). The SoG is followed by the five bilateral thoracic ganglia (T1-T5), located on either side of the SA, and the posterior-most ganglion, the abdominal ganglion (AG), which is also a fusion of multiple abdominal ganglia (Fig. 1A, B) (Bullock and Horridge, 1965; Sandeman and Atwood, 1982; Smarandache-Wellman, 2016). The TGM connects to the rest of the crustacean central nervous system via the large circumoesoesophageal connectives (*coc*s) at the anterior end of the SoG (Fig. 1A, B). The many additional nerves around the border of the TGM connect this structure to the pericardial organ, an endocrine structure surrounding the crab heart, and many other structures to send and receive information related to locomotion, respiration, digestive, and reproductive function (Bullock and Horridge, 1965; Harzsch, 2003; Sandeman and Atwood, 1982). The TGM is a relatively thick ganglion mass, with a dorsoventral depth of approximately 1 mm in crabs (Kornthong et al., 2014). This presents a challenge to performing detailed microscopic analysis of neurochemical distributions (Dircksen and Keller, 1988; Mangerich and Keller, 1988; Schmidt, 1997). Thus, our initial aim was to optimize our ability to identify and determine the size and axonal projections of potential endogenous TRP-IR cells. Both the soma diameter and the projection pathway can provide information about a potential cell type (Dircksen and Keller, 1988; Elson, 1996; Kornthong et al., 2014; Mangerich and Keller, 1988; Stephens, 1986; Yasuda-Kamatani and Yasuda, 2006).

A TRP-IR axon bundle was previously traced through the *coc*s to the SoG in TGMs that were compressed between a slide and coverslip. This study noted dense, intense TRP immunoreactivity in the TGM but did not include images or characterize this immunoreactivity (Blitz et al., 2008). In our initial examination of TRP immunoreactivity we used TGMs that were partially compressed to approximately half of the normal dorsoventral depth (0.5 mm) (compressed TGMs). We found extensive TRP immunoreactivity throughout the TGM (Fig. 1B), including the previously described TRP-IR axons in the *coc*s that entered into the SoG as in Blitz et al. (2008) (n=30, N=18). We also identified a bilateral pair of TRP-IR axon tracts projecting from anterior to posterior through the center of the SoG (n=23, N=13), then spreading apart to run around the perimeter of the SA toward the AG (n=5/5, N=3/3) (Fig. 1B). We refer to this centrally located tract as the TRP central tract (TRP_{CT}). The TRP_{CT} appeared to run through the ring commissure/longitudinal axon bundle which is a thick band of axons that runs along the dorsal-medial aspect of the sternal artery (Dircksen and Keller, 1988; Kornthong et al., 2014; Saetan et al., 2013). There was also TRP-IR neuropil located lateral to each TRP_{CT} along the length of the SoG (n=12, N=6) (Fig. 1B-C), in all of the T-ganglia (n=7-9, N=4-6) (Fig. 1B, D-H) and along both lateral margins of the AG (n=12, N=6) (Fig. 1B, I).

Although compression allowed us to identify major aspects of TRP immunoreactivity in the TGM, we were concerned that compressing the tissue could distort TRP-IR structures and their 3-D relationships. Therefore, we tried mounting TGMs without compression in 1 mm wells (uncompressed TGMs). This approach greatly diminished the visibility and clarity of TRP immunoreactivity. For example, the TRP_{CT} became more difficult to follow beyond the anterior SoG (Fig. 2Aii), cell bodies were more difficult to visualize (Fig. 2B-C), and the clarity of fine detail was poor (Fig. 2A-B) as detailed below. We thus needed a technique that both protected the anatomy of the TGM and improved resolution of immunoreactive structures throughout the thick, opaque TGM tissue.

We decided to employ a methyl-salicylate clearing technique which is routinely used to reduce tissue opacity by replacing water with methyl-salicylate (see Section 2.4) (Amos and Mesce, 1994; Bucher, 2014; Kononenko et al., 2018; Nässel, 1984; Thorn et al., 2007; Zucker et al., 2000). Although there was no statistical difference in visibility of the TRP_{CT} in the anterior SoG across mounting protocols (Fig. 2A) (compressed: 100%, n=23, N=13; uncompressed: 88%, n=16/18, N=8/9; cleared: 100%, n=20, N=10; Fisher's Exact Test, Bonferroni Correction, p=0.236-0.618), there were differences progressing posteriorly along the TGM. The TRP_{CT} was visible through the entire SoG, along the ipsilateral side of the sternal artery, and into the AG in all compressed TGMs (n=5/5, N=3/3) and all cleared TGMs (Fig. 3) (n=9/9, N=7/7), but only visible from the SoG to the AG in 50% of uncompressed TGMs (n=3/6, N=2/5). In the remaining uncompressed TGMs, the TRP_{CT} typically became too difficult to follow beyond T2 (n=3/6, N=3/5) (Fig. 2A) (Compressed vs. Uncompressed: p=0.031; Compressed vs. Cleared: p=1.00; Uncompressed vs. Cleared: p = 0.009; Fisher's Exact test, Bonferroni correction, $\alpha = 0.017$). Thus, the clearing protocol that we adapted to the crab TGM enabled more consistent tract tracing compared to uncompressed TGMs. Further, clearing the tissue did not appear to impact fine immunoreactive structures, as there was extensive neuropil labeling in all ganglia in cleared TGMs similar to compressed TGMs, and fine branches were evident between the TRP_{CT} and the regions of neuropil (SoG, AG: n=5, N=5; T1-T5, n=10, N=5) (Figs. 2, 3).

We examined somata in an anterior (thick) and a posterior (thin) location in TGMs to compare the visibility and numbers of somata across mounting protocols. In the SoG, which is one of the thicker ganglia of the TGM (~ 800 μm; Kornthong et al., 2014), there was a pair of TRP-IR cells in the anterior-medial SoG in 75% of compressed specimens (N=9/12) (Fig. 2Bi), 33% of uncompressed preparations (N=2/6) (Fig. 2Bii) and 100% of cleared specimens (N=7/7; Fig. 2Biii). Thus, the paired SoG cells were visible in more compressed than uncompressed TGMs (Fisher's Exact test, Bonferroni correction, p<0.001) and in more cleared than uncompressed TGMs (p<0.001) but in similar numbers of compressed and cleared TGMs (p=0.208). In the thinnest part of the TGM, the AG (~300 μm; Kornthong et al., 2014), neurons were consistently visible in compressed (N=6/6, Fig. 2Ci), uncompressed (N=9/9, Fig. 2Cii), and cleared TGMs (N=10/10, Fig. 2Ciii). Thus, we turned to counting the number of neurons per AG in order to assess if our clearing technique increased our ability to visualize cells, even in the thinnest part of the TGM. There were more cells in compressed (8 ± 1.9; N=6) and cleared (9.3 ± 2.4; N=10) ganglia than in uncompressed (3.9 ± 1.4; N=9) ganglia (One Way ANOVA, compressed vs uncompressed: p=0.003, cleared vs uncompressed: p<0.001), but no difference between cleared and compressed ganglia (p=0.235) (Fig. 2E). Due to the thickness of the TGM, we needed to extend the duration of the dehydration/rehydration steps (Section 2.4) compared to previous protocols that we used as a starting point (Bucher, 2014; Thorn et al., 2007; Zucker et al., 2000). Thus, we also wanted to determine whether this longer duration clearing process was distorting the tissue. We reasoned that the measures of AG cells in uncompressed TGMs were the most accurate. AG cell horizontal and vertical diameters were 59.42 ± 7.12 μm and 81.66 ± 10.32 μm in uncompressed preparations (N=9), 70.03 μm ± 5.99 μm and 104.08 μm ± 13.02 in compressed ganglia (N=6), and 54.33 ± 3.24 μm and 72.60 μm ± 7.90 μm in cleared TGMs (N=10) (Fig. 2F). The horizontal and vertical diameters of AG cells in compressed TGMs were larger than in uncompressed (One Way ANOVA, horizontal p=0.003, vertical p<0.001) and cleared TGMs (horizontal p<0.001, vertical p<0.001) (Fig. 2C, F). However, the AG cells in cleared TGMs were not different from those in uncompressed (horizontal diameter, p=0.059; vertical diameter, p=0.065) (Fig. 2F). Thus, our clearing method did not distort the anatomy of TRP-IR cells in the TGM, but compressing TGMs did cause distortion. We predict that we identified the low end of distortion that can be caused by compression as the AG is the ganglion with the smallest dorsoventral depth and therefore should be subjected to the least amount of compression. Eliminating size distortion is important for placing TRP-IR cells in previously determined size classes (Dircksen and Keller, 1988; Khornchatri et al., 2015; Kornthong et al., 2014; Saetan et al., 2013; Senarai et al., 2016).

3.2. TRP-IR cells in the SoG and AG

Using our modified clearing protocol, we examined the entire TGM for TRP-IR cell bodies that could contribute to paracrine and/or endocrine release of this signaling molecule. For all identified cells, the horizontal diameters were used to assign cells to size classes based on the classification of crustacean neurons used in Kornthong et al. (2014) (see Section 2.6). As noted above, a pair of cell bodies was consistently identified in the SoG (Fig. 2). The average horizontal and vertical diameter of the SoG neurons in cleared TGMs was 39.00 ± 2.67 µm and 49.30 ± 2.70 µm, respectively (n=12, N=6). Based on horizontal diameter, 9/12 (75%) of these neurons were in the large size class, and 3/12 (25%) were just below the cutoff and fell within the medium size class (Fig. 2G) (Table 1). As evident by tracing them through z-stacks of optical sections, SoG cell primary neurites projected posteriorly and appeared to contribute to an area of neuropil located at the midline (Fig. 2Biii) (n=12, N=6), but we were unable to trace them beyond this neuropil region. This pair of neurons were the only TRP-IR cells in the SoG and likely do not contribute to all of the neuropil within the SoG.

As indicated above, ~9 AG cells were visible in cleared TGMs (Fig. 2E) which had horizontal diameters that placed them primarily into the large size class (n=86/87, N=10) with the exception of one neuron classified as medium (n=1/87, N=10) (Fig. 2G) (Table 1). Many cells were located near the posterior end of the AG. However, several were along the anterior-posterior axis of the AG (Fig. 4). In cleared, uncompressed ganglia we were able to discern the relationship of the AG cells, their axons, and the AG neuropil to each other dorsoventrally in 3D space. A color depth code demonstrates that most of the AG neurons were ventral to the AG neuropil but some, especially the posterior neurons, were on a similar level as the AG neuropil or ventral to it (N=6, Fig. 4D). In cleared preparations, individual AG cell primary neurites were readily identifiable (Fig. 4). We found that single primary neurites crossed to the contralateral side of the ganglion close to their somata before proceeding anteriorly towards the sternal artery (N=6, Fig. 4B-C). The AG cell primary neurites did not appear to contribute to any neuropil in the AG (N=6, Fig. 4B-C). As noted above, the bilateral TRP_{CT} continue as central tracts running the length of the AG (Figs. 3, 5) and branches project from this continuation of the TRP_{CT} laterally toward the regions of neuropil (n=5, N=5) (Fig. 5B).

To gain further insight into their potential roles, we traced the AG cell axons. Continuing beyond the AG, individual AG cell axons projected up to T1 (N=4, Fig. 5) but we were unable to consistently trace them farther. In a single preparation, an AG cell axon was evident projecting beyond T1 (white arrows; Fig. 5C), but was lost as it entered the SoG. Although one possibility was that the AG cell axons merged with the TRP_{CT}, we found instead that they remained lateral to the TRP_{CT}, and primarily on a different dorsal-ventral plane. The bulk of the TRP_{CT} was more dorsal than the AG cell axons through T5-T3 but was more ventral beginning around T2. Due to their different dorsal-ventral planes and the extent of TRP immunoreactivity it is difficult to visualize the thin AG cell axons in a maximum intensity projection from a complete confocal z-stack (Fig. 5B). To allow comparison of their locations, maximum intensity projection images from a complete z-stack that includes the TRP_{CT} and from a partial z-stack that includes the AG cell axon, but not the TRP_{CT} are presented. The circles indicate the same x-y location in the full (Fig. 5B) and partial (Fig. 5C) z-stack to provide reference points. The AG cell axons remained lateral to the TRP_{CT} and were continuing to project toward the anterior edge of T1 away from the sternal artery, at the point when we were no longer able to trace them (Fig. 5C). These data suggest that the AG cell axons do not merge with the central TRP-IR tract, but may project out of the TGM through nerves in T1 or the SoG. Thus, in the SoG and AG there are primarily large size class TRP-IR neurons. SoG neurons may contribute to a central region of SoG neuropil, while AG neurons appear to project most of the distance of the TGM without contributing to neuropil. We next looked for additional TRP-IR somata in the remainder of the TGM.

3.3. TRP-IR cells throughout the T1-T5 region

TRP-IR cells were located in each of the T1-T5 ganglia (Fig. 6) (Table 1). The number of cells ranged from a consistent population of 3 neurons in T1, T2 and T4 to an average of 5 and 9 cells in T3 and T5 respectively (Fig. 6) (Table 1). Among the largest population in T5, there were isolated neurons (4 ± 1) as well as cells arranged in a cluster (6 ± 1 cells) (n=7, N=4) (Fig. 6B; T5, arrows). The cells in T1-T5 were primarily large and medium class cells based on their horizontal diameters, with a few small cells also located in T3 (5/35 cells, n=2/7, N=2/4) (Fig. 6C) (Table 1). We used the TRP_{CT} and its branches into the T-ganglia as references for the location of TRP-IR somata. Specifically, we noted whether T1-T5 cells were dorsal or ventral to the TRP_{CT}, and anterior or posterior to the TRP_{CT} branches in each ganglion (see Section 2.6). Most cells were located ventral to the central TRP-IR tract with the exception of some cells in T3 (8/35 cells, n=7, N=4) (Fig. 6B) (Table 2). There was less consistency in the relative anterior-posterior location of somata in T1-T5 (Table 2). Throughout T1-T5, no connections from the primary neurites of TRP-IR cells to the TRP_{CT} were observed (n=7, N=4). In the TGM, cell bodies are located not only within individual ganglia, but also between them (Mangerich and Keller, 1988; Saetan et al., 2013; Senarai et al., 2016). Thus, we also explored the regions between the ganglia for TRP-IR cells.

The regions between ganglia are referred to by their bordering ganglia. For example, the area between T1 and T2 is T1:T2 (Fig. 7A). The number of TRP-IR cells varied between ganglia and included varying percentages of cells in the large, medium, and small size classes (Fig. 7) (Table 3). The between ganglia cell numbers ranged from 0 for SoG:T1 (N=4), to an average of 10 cells in the T2:T2 region. Just anterior to the SA there is a non-bilateral commissure between the right T2 and the left T2 (T2R:T2L, Fig. 7A, B) (Bullock and Horridge, 1965; Harzsch, 2003; Sandeman and Atwood, 1982). All of the cells within this commissure were close to the SA (N=4, Fig. 7B). Based on their horizontal diameters, these cells fell in the small and medium class, and they did not have visible axons (n=40 cells, N=4, Fig. 7B, C) (Table 3). Across all intra- and inter-ganglia regions, T2R:T2L contained the only population of cells that did not include large size class cells.

No TRP-IR branches projected into the spaces between each of the ganglia, thus the depth of the inter-ganglionic cells was compared to depth at which the TRP branch in the ganglion closest to the most cells entered the TRP_{CT} (see Section 2.6). Most of the inter-ganglia cells were ventral to their respective intra-ganglion TRP-IR branch (92-100%; n=7-8; N=4) (Table 4). None of the inter-ganglia cell axons had visible connections with the TRP_{CT} (n=7-8; N=4).

4. Discussion

Using cleared tissue and confocal microscopy, we found TRP-IR tracts that projected the length of the TGM, neuropil in all ganglia, and ~110 cell bodies distributed within and between ganglia comprising the fused TGM of the crab, *C. borealis* (Fig. 8).

Due to the thickness and size of the TGM, compression or sectioning has been used with various labeling protocols to describe the TGM anatomy (Blitz et al., 2008; Bullock and Horridge, 1965; Dircksen and Keller, 1988; Khornchatri et al., 2015; Kornthong et al., 2014; Schmidt, 1997). We found that in compressed TGMs, the diameters of large TRP-IR neurons in the posterior AG were ~20-30% (horizontal-vertical) larger than in uncompressed TGMs. The AG has the smallest dorsal-ventral extent within the TGM (Kornthong et al., 2014; Saetan et al., 2013) and therefore is subject to the least compression, suggesting that greater distortion is likely in other TGM regions. Sectioning of tissue can avoid distortion due to compression and can be useful for characterizing anatomical structures, such as cell clusters throughout the TGM (Kornthong et al., 2014; Saetan et al., 2013). However, a downside to sectioning is the difficulty in reconstructing tissue, particularly a large structure such as the TGM, in order to trace axons outside the extent of individual sections and maintain three-dimensional spatial information.

Clearing techniques are routinely used to decrease the opacity of tissue and thus the light scatter that decreases detection of immunofluorescence (Amos and Mesce, 1994; Carrow et al., 1984; Nässel, 1984; Richardson and Lichtman, 2015; Seo et al., 2016; Silvestri et al., 2016; Vigouroux et al., 2017). Combining a clearing technique with confocal microscopy enables detection even in thicker tissues, thus making it feasible to maintain three-dimensional anatomy and trace processes without the need for reconstruction (Richardson and Lichtman, 2015; Seo et al., 2016; Silvestri et al., 2016; Vigouroux et al., 2017). Several clearing protocols improve visibility in thick tissue and still enable fluorescence confocal imaging. However, there is variability in the efficacy of protocols across tissues, including differences in distortion (Richardson and Lichtman, 2015; Seo et al., 2016; Zucker et al., 2000). Methyl salicylate protocols preserve morphology better than others, including mounting in glycerol (Bucher, 2014; Zucker et al., 2000). Further, methyl salicylate clearing works with whole-mounted tissues (up to 2 mm), including preserving morphology in whole-mounted insect and embryonic mouse tissues (Amos and Mesce, 1994; Carrow et al., 1984; Zucker et al., 2000). Optimizing a methyl salicylate clearing protocol for the TGM (Bucher, 2014; Zucker et al., 2000) improved our ability to detect TRP-IR structures, including axons and cell bodies throughout the crab TGM without distortion. Other anatomical studies of the TGM of short bodied crustaceans cite difficulty visualizing or a failure to trace axons very far (Dircksen and Keller, 1988; Mangerich and Keller, 1988; Schmidt, 1997). While we were still unable to trace axons to their terminals, the optimized clearing technique allowed us to trace axons of AG cells through ~ 80% of the length of the TGM without the need to section and reconstruct this large, fused ganglion mass.

The distribution of TRP-IR somata has been assessed in the STNS and supraoesophageal ganglion of some decapod crustaceans (Blitz et al., 1995; Goldberg et al., 1988; Yasuda-Kamatani and Yasuda, 2006) but, to our knowledge, an anatomical analysis of TRP-IR somata in the TGM of a decapod has not been conducted. Previous examination of TRP immunoreactivity in the lobster *Hommarus americanus* focused on sensory afferents entering the TGM (Schmidt, 1997). Here, we characterized the distribution of the major TRP-IR structures and in particular, TRP-IR somata in the TGM of *C. borealis*.

4.1. TRP immunoreactivity in the SoG

The SoG controls appendages in the mouth area including the labrum, mandible, maxilla 1 and 2 and maxilliped 1-3 (Bullock and Horridge, 1965; Harzsch, 2003; Harzsch et al., 1998; Robertson and Laverack, 1979; Saetan et al., 2013; Wales et al., 1976). Most of these are important for food intake. Thus, the two TRP-IR neurons or other extrinsic sources contributing to the TRP-IR neuropil in the SoG might modulate food intake. TRP modulates other feeding related behaviors, including chewing and food filtering within the foregut (Blitz et al., 2008; Diehl et al., 2013; Stein et al., 2007). Additionally, maxilla 2 controls the gill bailer and thus gas exchange via ventilation (Dicaprio, 1989; Pilkington and MacFarlane, 1978), which could also be modulated by TRP in the SoG. Similarly, the respiratory system in mammals is modulated by the most well-known tachykinin, the peptide Substance P (Doi and Ramirez, 2008; Peña and Ramirez, 2004).

4.2. TRP immunoreactivity in the T-ganglia

Most TRP-IR cells in the T-ganglia were located ventral to the TRP_{CT}, although a few in T3 and between T5 and the AG were located dorsally. The pattern of labeled somata appears to differ from cells that are immunoreactive for crustacean cardioactive peptide (CCAP), pigment dispersing hormone (PDH), FMRF-amide, Leu-enkephalin-like peptide, serotonin, and dopamine which are located on the dorsal side of the TGM in several crustacean species (Dircksen et al., 1987; Dircksen and Keller, 1988; Kornthong et al., 2014; Maynard, 1961). The exceptions are dopaminergic neurons between the T-ganglia on the ventral side of the TGM (Khornchatri et al., 2015); thus, in the future, cells could be examined for colocalization of dopamine and TRP. Colocalization of transmitters is prevalent in nervous systems, although it does not occur in all cells (Cropper et al., 2018; Nusbaum et al., 2017; Svensson et al., 2019). For example, a TRP-containing modulatory projection neuron in the STNS has a peptide and small molecule co-transmitter, while the ACO neuroendocrine organ appears to contain only TRP (Blitz et al., 1999; Messinger et al., 2005; Stein et al., 2007).

The five bilaterally paired T-ganglia provide input to, and receive sensory information from, the claws and legs (Bullock and Horridge, 1965; Elson, 1996; Stephens, 1986). TKs and TRPs modulate locomotion in several organisms including *Drosophila* and lamprey (Pérez et al., 2007; Winther et al., 2006) and the localization of TRP in neuropil and cells throughout the T-ganglia suggest a similar function in crabs. The TRP_{CT} has projections into all of the T-ganglia (this study), while TRP-IR sensory afferents project into T-ganglia from the periphery (Schmidt, 1997). In locusts, TRP-IR axons entering thoracic ganglia originate from sensory hairs on the tarsi of each leg (Persson and Nässel, 1999). Thus, TRP-IR neuropil within the T-ganglia may be predominantly sensory input to locomotor circuits.

We were unable to trace the TRP-IR cell axons in their entirety and thus could not determine if they were motor neurons or interneurons. Each cell type is plausible. Although small molecule transmitters such as glutamate and acetylcholine are typical transmitters at the neuromuscular junction, some motor neurons in invertebrates and vertebrates contain peptide co-transmitters (Cropper et al., 2018; Piehp et al., 1993; Rosenfeld et al., 1983; Vilim et al., 2000; Walder et al., 2013; Whim et al., 1993). Alternatively, many interneurons in vertebrates and invertebrates contain neuropeptides

(Baraban and Tallent, 2004; Nässel and Homberg, 2006), and interneurons that are part of rhythm generating circuits can be intrinsic sources of modulation to the circuit (Cropper et al., 2018; Katz and Frost, 1996).

4.3. TRP immunoreactivity in the AG

Our results suggest that there is no local TRP modulation in the AG, a region that controls reproductive and digestive functions (Bullock and Horridge, 1965; Kornthong et al., 2014; Sandeman and Atwood, 1982; Senarai et al., 2016). The TRP-IR cells in the AG were in the large size class which are proposed to be motor neurons (Kornthong et al., 2014). However, motor neurons typically innervate muscles in their segment (Bullock and Horridge, 1965), whereas the AG TRP-IR neurons in this study projected anteriorly to at least T1. In general, somata within the TGM are interneurons, motor neurons, or neurosecretory, with sensory somata typically located in the periphery (Bullock and Horridge, 1965). There appear to be both ascending interneurons and neurosecretory neurons originating in the AG that project several segments anteriorly. For instance, AG neurons immunoreactive for CCAP in the green crab *C. maenas* project their axons ipsilaterally and anteriorly to the SoG, and then leave through segmental nerves projecting to the pericardial organ (PO) (Dircksen and Keller, 1988). The PO is one of the major neuroendocrine organs in crustaceans and it does release TRP in *C. borealis* (Christie, 2011; Li et al., 2003), raising the possibility that the TRP-IR AG neurons project to the PO. Given their large size, and lack of any branching as they project anteriorly it is perhaps more likely that AG cells are neuroendocrine and release TRP from the PO organ into the circulation, and do not have any local regulatory functions.

4.4. TRP_{CT}

The other major TRP-IR structure in the TGM is in the form of bilateral longitudinal axon tracts, the TRP_{CT}. There are thick longitudinal tracts that run lateral to the sternal artery through the entire fused ganglion mass of short-bodied crab species (Kornthong et al., 2014; Saetan et al., 2013). Other neuromodulators are present in subsets of these axons, including dopamine, CCAP, FMRFamide, and PDH (Dircksen and Keller, 1988; Khornchatri et al., 2015; Mangerich and Keller, 1988; Wood and Derby, 1996). These labeled axons appeared sparser than the TRP-IR axons in this study and thus are unlikely to be the same axons. There is no evidence for axons from TRP-IR somata in the TGM connecting to the TRP_{CT}. This includes the AG cells, which had axons that were traceable for a long distance, yet remained lateral to the TRP_{CT}. Thus, the cell bodies from which the TRP_{CT} axons originate likely occur outside the TGM, and thus may be sensory or neuroendocrine.

4.5. Neuroendocrine Release

Hormonal TKs and TRPs modulate aggression, reproduction, and hunger/satiety (Chen et al., 2010; De Felipe et al., 1998; Harrison and Geppetti, 2001; Kahsai et al., 2010; Nässel et al., 2019). In crustaceans, hormonal TRPs modulate heartbeat, gastric-mill muscles, gut motility, and feeding state (Chen et al., 2010; Christie et al., 1997; Cruz-Bermúdez and Marder, 2007; Messinger et al., 2005). Endocrine sources of TRP vary across crustacean species with the PO, ACO and midgut epithelial cells being known sources in *C. borealis* (Christie, 2011; Christie et al., 2007; Li et al., 2003; Messinger et al., 2005). The thoracic ganglion mass may serve as yet another source of hormonal TRP.

There are multiple potential sites at which hormones can be released into the circulation from TGM neurons. For instance, in the lobster *H. americanus* ventral nerve cord 5HT and OCT neurons arborize within ganglia where they can act via paracrine release, and they project to thoracic nerve roots where they form neurosecretory plexi (Heinrich et al 2000, Schneider et al 1993). Although, much neuroendocrine release occurs at axon terminals, release from somata also occurs, including in the TGM (Matsumoto, 1954; Maynard, 1961). The cells near the sternal artery in the T2:T2 commissure without evident axons, appear similar to B-type neurosecretory cells near the sternal artery in the crabs *Portunus pelagicus* and *Eriocheir japonicus* (Matsumoto, 1954; Stewart et al., 2013). It is also possible that TRP could be released from cells scattered in other areas of the TGM to enter the circulation, as the TGM is fenestrated with capillaries and hemolymph lacunae, including individual neuroendocrine cells having capillaries wrapped around their somata (Matsumoto, 1954; McGaw, 2005;

McGaw and Reiber, 2002). Other than the AG cell axons, we were unable to trace axons very far, and unable to trace any axons to their terminations. Therefore, determination of potential endocrine or dual neuronal/endocrine TRP release in the TGM will require other approaches, such as single cell fills that enable an assessment of the full arborization of cells (Blitz et al., 1999; Dicaprio, 1989; Heinrich et al., 2000).

5. Conclusions

We established that a crustacean TRP is highly expressed in the third major component of the crustacean CNS, the TGM, in addition to the supraoesophageal ganglion and the STNS. The large number of intrinsic sources of TRP from local cells likely extends the functions of TRP to local modulation of circuits controlling food intake, locomotion, and ventilation in *C. borealis.* Further work is necessary to identify extrinsic origins of TRP to the TGM, such as the location and type of cells from which the TRP_{CT} axons originate. Beyond local release, the TGM is a potential additional site of hormonal TRP release. One potential trigger for hormonal TRP release could be sensory feedback from the mouthparts, which project into the SoG where there is extensive TRP immunoreactivity. This fits well with the rise in TRP that occurs in fed crabs and the ability of mammalian TKs to suppress food intake (Chen et al., 2010, 2009b; Kalra et al., 1991; Lin et al., 2000). TRP actions may also have downstream effects beyond the TGM due to extensive projections between the TGM and the other major CNS regions. Thus, understanding the distribution of TRP in the TGM is important for understanding its many roles in regulating crustacean physiology.

Acknowledgements

We thank Savanna-Rae Fahoum for helpful discussions and feedback on the manuscript.

Funding: Financial support for this study was provided by the National Science Foundation (IOS-1755283: DMB), Miami University Undergraduate Research Awards (KM, SMF, HMK) and the Department of Biology at Miami University.

Table 1. Counts and diameters of TRP-IR somata within ganglia of the TGM.

		Count per Cell Category[a]			Horizontal and Vertical Diameters per Cell Category (µm)[b]			
	Total Cell Count	Small	Medium	Large	Small	Medium	Large	n, N[c]
SoG	2.0 ± 0	0 ± 0	0.5 ± 0.6	1.5 ± 0.6	---	32.99 ± 1.45 46.24 ± 3.77	40.70 ± 1.97 50.06 ± 4.28	6
T1	3.0 ± 0	0 ± 0	1.8 ± 0.4	0.9 ± 0.3	---	26.59 ± 3.97 41.20 ± 7.27	79.18 ± 13.61 98.10 ± 18.24	8, 4
T2	3.0 ± 0	0 ± 0	1.5 ± 0.5	1.5 ± 0.5	---	25.13 ± 3.77 36.89 ± 6.21	43.65 ± 9.67 53.21 ± 11.37	8, 4
T3	5.0 ± 1.5	0.7 ± 1.2	1.7 ± 0.70	2.6 ± 1.1	15.25 ± 0.86 25.64 ± 4.46	27.30 ± 3.53 36.22 ± 8.45	44.39 ± 8.80 55.24 ± 11.02	7, 4
T4	3.0 ± 0	0 ± 0	0.6 ± 0.5	2.4 ± 0.5	---	32.62 ± 0.78 47.74 ± 6.74	49.60 ± 11.72 59.33 ± 13.00	7, 4
T5	9.4 ± 0.7	0 ± 0	6.4 ± 0.9	3.1 ± 1.3	---	25.46 ± 4.61 36.43 ± 6.75	42.40 ± 5.93 53.33 ± 9.42	7, 4
AG	9.3 ± 2.5	0 ± 0	0.1 ± 0.3	8.6 ± 2.7	---	32.85 56.07	54.60 ± 10.46 71.81 ± 14.73	10

[a] There were no TRP-IR cells that were categorized as Globuli or Giant in any of the ganglia, thus these two categories were excluded from the table. [b] For each ganglion/cell class entry, the horizontal diameters are the upper numbers and the vertical diameters are the lower numbers in each set. [c] The number of ganglia (n) and the number of TGMs (N) analyzed are indicated for bilateral structures and only the number of TGMs for unilateral structures (SoG and AG). All data are presented as Mean ± SD.

Table 2. Somata locations within ganglia of the TGM relative to TRP_{CT} branches.

	# Ventral[a]	# Dorsal[a]	# Anterior[a]	# Posterior[a]	n, N[b]
T1	21	0	6	15	8, 4
T2	24	0	2	22	8, 4
T3	27	8	20	15	7, 4
T4	21	0	2	19	7, 4
T5	66	0	18	48	7, 4

[a] The number of cells that were ventral versus dorsal, and anterior versus posterior to the TRP_{CT} branches (see Section 2.6) in all analyzed ganglia are indicated. [b] The number of ganglia (n) and the number of TGMs (N) analyzed are indicated for the bilateral T1-T5 ganglia.

Table 3. Counts and diameters of TRP-IR somata between ganglia of the TGM.

	Count per Cell Category[a]				Horizontal and Vertical Diameters per Cell Category (μm)[b]			
	Total Cell Count	Small	Medium	Large	Small	Medium	Large	n, N[c]
SoG:T1	0 ± 0	---	---	---	---	---	---	8, 4
T1:T2	5.1 ± 0.6	0 ± 0	4.1 ± 0.6	0.9 ± 0.3	---	24.24 ± 4.49 32.64 ± 5.78	55.18 ± 9.32 74.39 ± 10.17	8, 4
T2R:T2L	10.0 ± 1.0	4.5 ± 1.1	5.5 ± 0.5	0 ± 0	14.47 ± 1.37 22.20 ± 3.73	22.65 ± 4.41 30.19 ±6.83	---	4
T2:T3	6.7 ± 1.4	0.1 ± 0.4	4.4 ± 1.2	2.1 ± 0.6	15.19 26.0	22.86 ± 3.91 32.81 ± 8.09	47.52 ± 9.31 64.35 ± 14.44	7, 4
T3:T4	1.9 ± 1.4	0.6 ± 0.5	1.0 ± 0.6	1.0 ± 0.6	13.94 ± 2.25 25.23 ± 7.48	24.6 ± 5.08 31.80 ± 5.71	38.1 ± 5.71 58.73 ± 19.90	7, 4
T4:T5	2.7 ± 0.5	0 ± 0	1.3 ± 0.7	1.4 ± 0.5	---	27.68 ± 5.52 39.71 ± 8.78	45.90 ± 8.71 57.24 ± 4.93	7, 4
T5:AG	3.4 ± 0.9	0 ± 0	0.6 ± 0.7	2.7 ± 0.7	---	25.21 ± 14.28 36.24± 20.47	46.82 ± 5.80 66.28 ± 9.68	7, 4

[a] There were no TRP-IR cells that were categorized as Globuli or Giant between any of the ganglia, thus these two categories were excluded from the table. [b] For each ganglion/cell class entry, the horizontal diameters are the upper numbers and the vertical diameters are the lower numbers in each set. [c] The number of between ganglia regions (n) and the number of TGMs (N) analyzed are indicated for bilateral structures and only the number of TGMs for unilateral structures (T2R:T2L). All data are presented as Mean ± SD.

Table 4. Somata locations between ganglia of the TGM relative to the nearest TRP_{CT} branches.

	# Ventral[a]	# Dorsal[a]	Boundary Ventral-Dorsal[a]	TRP_{CT} Ganglion[b]	n, N[c]
T1:T2[d]	41	0	0	T2	8, 4
T2R:T2L	38	0	2	T2	4
T2:T3	47	0	0	T3	7, 4
T3:T4	13	0	0	T4	7, 4
T4:T5	19	0	0	T5	7, 4
T5:AG	22	2	0	T5	7, 4

[a] The number of cells that were ventral versus dorsal to, or at the same dorsal-ventral depth as the TRP_{CT} branches (see Section 2.6) across all analyzed ganglia are indicated. [b] The ganglion with the closest TRP_{CT} that was used for analysis is listed. [c] The number of between ganglia areas (n) and the number of TGMs (N) analyzed are indicated for the bilateral T1-T5 ganglia. [d] There were no TRP-IR cells identified in the SoG:T1 region, therefore it was not included in this table.

Figure Legends

Figure 1. There is dense TRP immunoreactivity throughout the crab TGM. A) A schematic of the TGM which includes a single SoG at the anterior end, a fused AG at the posterior end, and the bilaterally symmetrical thoracic ganglia 1-5 (T1-T5) surrounding the sternal artery (SA). The *coc*s connect the TGM to the remainder of the crab central nervous system. B) A maximum intensity projection of a 5 x 17 tile of single optical sections (86.83 µm optical section) of an entire compressed TGM, illustrates a bilateral set of TRP-IR axon tracts (TRP_{CT}, open arrows) and neuropil throughout the TGM. A population of TRP-IR axons enters the anterior SoG from the *coc*s (Blitz et al., 2008). Scale bar is 1 mm. C-I) Digitally magnified sections from the image in (B) illustrate the presence of TRP-IR neuropil in all ganglia of the TGM. Scale bar in (C-I) is 200 µm. Abbreviations: AG, abdominal ganglion; *coc*s, circumoesophageal connectives; SA, sternal artery; SoG, suboesophageal ganglion; T1-T5, thoracic ganglia 1-5.

Figure 2. Clearing improved visibility of TRP-IR structures without distortion. The visibility of TRP_{CT} axons (A) and cell bodies in the SoG (B) and AG (C) were compared between compressed, uncompressed and cleared preparations. Ai) In the anterior SoG of compressed TGMs, the bilateral TRP_{CT} axons (arrowheads) were visible from the anterior to the posterior SoG (maximum intensity projection; 29 optical sections, 6.76 µm per optical section). Aii) In an uncompressed preparation, the TRP_{CT} was visible (arrowheads) in the anterior portion but becomes difficult to follow toward the posterior end of the SoG. Additionally, little other TRP immunoreactivity was visible (27 optical sections, 6.76 µm per optical section). Aiii) The TRP_{CT} axons were clearly visible (arrowheads) along the length of the SoG in a cleared TGM. Further, the neuropil was more distinct and TRP-IR branches were visible projecting from the TRP_{CT} toward the lateral margins of the SoG (maximum intensity projection, 12 optical sections, 37.09 µm per optical section). Scale bars: 100 µm. B) A pair of TRP-IR cell bodies was visible, although fuzzy, between the bilateral TRP_{CT} in a compressed TGM (Bi, arrows) but barely visible (arrows) in an uncompressed TGM (Bii). In contrast, in a cleared TGM,

these somata (Biii, arrows) were clearly visible, including their nuclei, and the primary neurites (arrowheads) could be followed from the cell body toward a posterior region of neuropil. Also note the improved clarity of the TRP_{CT} axon tracts to either side of the cell bodies. Scale bars are 100 µm. C) A single TRP-IR somata was 77 µm in a compressed TGM (Ci), 58 µm in an uncompressed TGM (Cii), and three somata were 58-62 µm in a cleared TGM (Ciii). Scale bars: 100 µm. D) A TGM schematic highlights the regions (boxes) used for comparison of TRP immunoreactivity across mounting protocols in A-C. E) The average number of visible TRP-IR cell bodies in the AG is plotted for compressed (white bar), uncompressed (grey bar), and cleared (black bar) preparations. F) The average horizontal and vertical diameters of TRP-IR cells in the AG in compressed (white bars), uncompressed (grey bars), and cleared (black bars) TGMs are plotted. G) Cells within the SoG and AG fall primarily in the large size class based on horizontal diameter, with a small number of medium cells in the SoG. AG: N=10; SoG: N=6. *p<0.05, **p<0.001. One-Way ANOVA with post hoc Holm-Sidak analysis.

Figure 3. The TRP_{CT} projects the entire length of the TGM with branches into all ganglia of the TGM. A) The complete projection of the bilateral TRP_{CT} (open arrows) from the SoG, around the sternal artery and entering into the AG is visible in a maximum intensity projection of a tiled set of z-stack (12 optical sections, 37.09 µm per optical section) confocal images of a cleared TGM. Scale bar is 1 mm. B-H) Digital zoom of regions from all ganglia from the tiled images in (B) highlights the TRP_{CT} (open arrows) as it passes through and branches (filled arrows) into each ganglion. Scale bars are 200 µm.

Figure 4. AG somata are distributed throughout the dorsal-ventral axis of the AG and have contralaterally projecting axons. A) Box on schematic indicates the area of images in (B-D). B) In the middle of the AG in a cleared preparation, two AG cells and

their respective axons were clearly visible. The axons of each cell (closed or open arrows) projected across the neuropil region to the contralateral side of the AG (20x maximum intensity projection, 188 optical sections, 1.04 µm per optical section). C) In a cleared TGM, axons from AG cells (arrows) projected anteriorly toward T5. (maximum intensity projection, 1x2 tile, 13 optical sections, 35.80 µm per optical section). Di) A 3D rendering from a confocal z-stack with a color depth code applied indicates the relative dorsal-ventral locations of cells and neuropil. Dii) The 3D rendering in Di was rotated 90 degrees. Although the side view is not as crisp as the top down view due to limitations of the computer rendered 3D image, it is clear that that several cells are located ventral to the neuropil with others located at a similar dorsal-ventral extent as the AG neuropil. (3D rendering, original z-stack 37 optical sections, 6.87 um per optical section). The color code at the bottom of the figure applies to Di and Dii. Scale bar for all images: 100 µm.

Figure 5. AG cell axons projected from AG to at least T1, lateral to the TRP_{CT}. A) Boxes on the schematic indicate the locations of images in B-C. B) In a montage of maximum intensity projections (15-25 optical sections per z-stack, 6.87 µm per optical section) from a cleared TGM, the TRP_{CT} projects from the AG to the SoG, near the edge of the sternal artery. The circles mark points along the TRP_{CT} used for reference in (C). A subset of optical sections from (B) (maximum projections of 3-9 optical sections per z-stack, 6.87 µm per optical section), in which a single AG axon was visible from the AG to T1 (arrows), was used to generate the montage in (C). It was not possible to follow the axon beyond the entrance to the SoG. The AG axon was lateral to the TRP_{CT} (circles) from the AG to T1. Scale bar: 100 µm.

Figure 6. TRP-IR cells were present in T1-T5 ganglia. A) The boxes on the TGM schematic show the location of images in (B). B) TRP-IR somata (arrows) were found in T1-T5. Most cells had a visible primary neurite projecting from the cell body. Almost all cells were located ventral to the TRP_{CT} with the exception of a subset of cells in T3 (T3dorsal; see Table 2). The number and sizes of cells varied across the ganglia (see Table 1), with most cells falling into the medium and large size classes (C) (n=7-8,

N=4). (maximum intensity projections, 4-8 optical sections per z-stack, 6.87 µm per optical section). Each scale bar is 100 µm.

Figure 7. TRP-IR cells were present between most ganglia. A) The boxes on the TGM schematic show the location of images in (B). B) TRP-IR somata (arrows) occurred in between ganglia of the TGM and within the commissure between T2 right and T2 left (T2R:T2L). Similar to cells within ganglia, most cells between ganglia had visible primary neurites projecting from the cell body, with the exception of small cells in the T2R:T2L commissure, which runs close to the SA. (maximum intensity projections, T1:T2 to T4:T5: 2-17 optical sections per z-stack, 6.87 µm per optical sections; T5:AG: 5 optical sections, 7.04 µm per optical section). Each scale bar is 100 µm. C) Cells in between ganglia mostly fell within the large and medium class sizes, although there were more small cells between ganglia, than within ganglia, particularly in the T2R:T2L commissure (n=7-8, N=4).

Figure 8. TRP immunoreactivity occurred throughout the TGM. A TGM schematic summarizes the locations of TRP-IR somata throughout the TGM. Only 2 cells were consistently found in the SoG, ~2-10 cells were found within and between T ganglia, and ~9 cells were found in the AG. A bilateral axon tract, the TRP_{CT} ran the entire length of the TGM, with branches into all ganglia. In the SoG and AG, there were bilateral regions of neuropil to either side of the TRP_{CT} as well as neuropil in the bilateral T1-T5 ganglia.

Literature Cited

Amos, T. M., Mesce, K.A., 1993. Reorganization of the ventral nerve cord in the moth *Manduca sexta* (L.) (lepidoptera:sphingidae). Int. J. Insect Morphol. & Embryol. 23, 21-37.

Baraban, S.C., Tallent, M.K., 2004. Interneuron Diversity series: Interneuronal neuropeptides - Endogenous regulators of neuronal excitability. Trends Neurosci. https://doi.org/10.1016/j.tins.2004.01.008

Blitz, D.M., Christie, A.E., Coleman, M.J., Norris, B.J., Marder, E., Nusbaum, M.P., 1999. Different proctolin neurons elicit distinct motor patterns from a multifunctional neuronal network. J. Neurosci. 19, 5449–5463. https://doi.org/10.1523/jneurosci.19-13-05449.1999

Blitz, D.M., Christie, A.E., Marder, E., Nusbaum, M.P., 1995. Distribution and effects of tachykinin-like peptides in the stomatogastric nervous system of the crab, *Cancer borealis*. J Comp Neurol 354, 282–294.

Blitz, D.M., White, R.S., Saideman, S.R., Cook, A., Christie, A.E., Nadim, F., Nusbaum, M.P., 2008. A newly identified extrinsic input triggers a distinct gastric mill rhythm via activation of modulatory projection neurons. J. Exp. Biol. 211, 1000–1011. https://doi.org/10.1242/jeb.015222

Bucher, D., 2014. Mounting and Clearing the STG for Microscopy [www Document]. URL http://www.bio.brandeis.edu/marderlab/microscopy3.html

Bullock, T.H., Horridge, G.A., 1965. Structure and function in the nervous systems of invertebrates, in: Structure and Function in the Nervous Systems of Invertebrates. Freeman, San Fransicsco. https://doi.org/10.1016/0013-4694(66)90114-3

Buma, P., Roubos, E.W., 1986. Ultrastructural demonstration of nonsynaptic release sites in the central nervous system of the snail *Lymnaea stagnalis*, the insect *Periplaneta americana*, and the rat. Neuroscience 17, 867–879. https://doi.org/10.1016/0306-4522(86)90051-5

Carrow, G.M., Calabrese, R.L., Williams, C.M., 1984. Architecture and physiology of insect cerebreal neurosecretory cells. J Neurosci. 4, 1034-1044.

Chen, R., Hui, L., Cape, S.S., Wang, J., Li, L., 2010. Comparative neuropeptidomic analysis of food intake via a multifaceted mass spectrometric approach. ACS

Chem. Neurosci. 1, 204–214. https://doi.org/10.1021/cn900028s

Chen, R., Hui, L., Sturm, R.M., Li, L., 2009a. Three dimensional mapping of neuropeptides and lipids in crustacean brain by mass spectral imaging. J. Am. Soc. Mass Spectrom. 20, 1068–1077. https://doi.org/10.1016/j.jasms.2009.01.017

Chen R., Ma, M., Hui, L., Zhang, J., Li, L., 2009b. Measurement of neuropeptides in crustacean hemolymph via MALDI mass spectrometry. J Am Soc Mass Spectrom. 20, 708-718. https://doi.org/10.1016/j.jasms.2008.12.007

Chowanski, S., Adamski, Z., Lubawy, J., Marciniak, P., Pacholska-Bogalska, J., Slocinska, M., Spochacz, M., Szymczak, M., Urbanski, A., Walkowiak-Nowicka, K., Rosinski, G., 2017. Insect Peptides - Perspectives in Human Diseases Treatment. Curr. Med. Chem. 24, 3116–3152. https://doi.org/10.2174/0929867324666170526120218

Christie, A.E., 2011. Crustacean neuroendocrine systems and their signaling agents. Cell Tissue Res. 345, 41–67. https://doi.org/10.1007/s00441-011-1183-9

Christie, A.E., Chi, M., Lameyer, T.J., Pascual, M.G., Shea, D.N., Stanhope, M.E., Schulz, D.J., Dickinson, P.S., 2015. Neuropeptidergic signaling in the american lobster *Homarus americanus*: New insights from high-throughput nucleotide sequencing. PLoS One 10. https://doi.org/10.1371/journal.pone.0145964

Christie, A.E., Kutz-Naber, K.K., Stemmler, E.A., Klein, A., Messinger, D.I., Goiney, C.C., Conterato, A.J., Bruns, E.A., Hsu, Y.W.A., Li, L., Dickinson, P.S., 2007. Midgut epithelial endocrine cells are a rich source of the neuropeptides APSGFLGMRamide (*Cancer borealis* tachykinin-related peptide Ia) and GYRKPPFNGSIFamide (Gly^1-SIFamide) in the crabs *Cancer borealis, Cancer magister and Cancer productus*. J. Exp. Biol. 210, 699–714. https://doi.org/10.1242/jeb.02696

Christie, A.E., Lundquist, C.T., Nässel, D.R., Nusbaum, M.P., 1997. Two novel tachykinin-related peptides from the nervous system of the crab *Cancer borealis*. J. Exp. Biol. 200, 2279–2294.

Christie, A.E., Skiebe, P., Marder, E., 1995. Matrix of neuromodulators in neurosecretory structures of the crab *Cancer borealis*. J. Exp. Biol. 198, 2431–2439.

Christie, A.E., Stemmler, E.A., Dickinson, P.S., 2010. Crustacean neuropeptides. Cell. Mol. Life Sci. 67, 4135–4169. https://doi.org/10.1007/s00018-010-0482-8

Cropper, E.C., Jing, J., Vilim, F.S., Weiss, K.R., 2018. Peptide cotransmitters as dynamic, intrinsic modulators of network activity. Front. Neural Circuits 12, 78. https://doi.org/10.3389/fncir.2018.00078

Cruz-Bermúdez, N.D., Marder, E., 2007. Multiple modulators act on the cardiac ganglion of the crab, *Cancer borealis*. J. Exp. Biol. 210, 2873–2884. https://doi.org/10.1242/jeb.002949

Cuello, A.C., Galfre, G., Milstein, C., 1979. Detection of substance P in the central nervous system by a monoclonal antibody. Proc Natl Acad Sci USA 76, 3532–3536.

Daur, N., Nadim, F., Bucher, D., 2016. The complexity of small circuits: the stomatogastric nervous system. Curr. Opin. Neurobiol. 41, 1–7. https://doi.org/10.1016/j.conb.2016.07.005

De Felipe, C., Herrero, J.F., O'Brien, J.A., Palmer, J.A., Doyle, C.A., Smith, A.J.H., Laird, J.M.A., Belmonte, C., Cervero, F., Hunt, S., 1998. Altered nociception, analgesia and aggression in mice lacking the receptor for substance P. Nature 392, 394–397.

Dicaprio, R.A., 1989. Nonspiking interneurons in the ventilatory central pattern generator of the shore crab, *Carcinus maenas*. J. Comp. Neurol. 285, 83–106. https://doi.org/10.1002/cne.902850108

Dickinson, P.S., Qu, X., Stanhope, M.E., 2016. Neuropeptide modulation of pattern-generating systems in crustaceans: comparative studies and approaches. Curr. Opin. Neurobiol. 41, 149–157. https://doi.org/10.1016/j.conb.2016.09.010

Diehl, F., White, R.S., Stein, W., Nusbaum, M.P., 2013. Motor circuit-specific burst patterns drive different muscle and behavior patterns. J. Neurosci. 33, 12013–12029. https://doi.org/10.1523/JNEUROSCI.1060-13.2013

Dircksen, H., Keller, R., 1988. Immunocytochemical localization of CCAP, a novel crustacean cardioactive peptide, in the nervous system of the shore crab, *Carcinus maenas* . Cell Tissue Res. 254, 347–360. https://doi.org/10.1007/BF00225807

Dircksen, H., Stangier, J., Keller, R., 1987. Proctolin-like, FMRFamide-like, and Leu-enkephalin-line immunoreactivity in the pericardial organs of brachyuran crustaceans. Gen Comp Endocrinol 66, 42.

Doi, A., Ramirez, J.M., 2008. Neuromodulation and the orchestration of the respiratory rhythm. Respir. Physiol. Neurobiol. 164, 96–104. https://doi.org/10.1016/j.resp.2008.06.007

Elson, R.C., 1996. Neuroanatomy of a crayfish thoracic ganglion: Sensory and motor roots of the walking-leg nerves and possible homologies with insects. J. Comp. Neurol. 365, 1–17. https://doi.org/10.1002/(SICI)1096-9861(19960129)365:1<1::AID-CNE1>3.0.CO;2-7

Goldberg, D., Nusbaun, M.P., Marder, E., 1988. Substance P-like immunoreactivity in the stomatogatric nervous systems of the crab, *Cancer borealis* and the lobsters *Panulirus interruptus* and *Homarus americanus*. Cell Tissue Res. 252, 515–522.

Harrison, S., Geppetti, P., 2001. Substance P. Int. J. Biochem. Cell Biol. 33, 555–576. https://doi.org/10.1016/s1357-2725(01)00031-0

Harzsch, S., 2003. Ontogeny of the ventral nerve cord in malacostracan crustaceans: a common plan for neuronal development in Crustacea, Hexapoda and other Arthropoda? Dev. Arthropod Nerv. Syst. a Comp. Evol. Approach 32, 17–37. https://doi.org/10.1016/S1467-8039(03)00008-2

Harzsch, S., Miller, J., Benton, J., Dawirs, R., Beltz, B., 1998. Neurogenesis in the thoracic neuromeres of two crustaceans with different types of metamorphic development. J. Exp. Biol. 201, 2465.

Heinrich, R., Bräunig, P., Walter, I., Schneider, H., Kravitz, E.A., 2000. Aminergic neuron systems of lobsters: Morphology and electrophysiology of octopamine-containing neurosecretory cells. J. Comp. Physiol. - A Sensory, Neural, Behav. Physiol. 186, 617–629. https://doi.org/10.1007/s003590000116

Huybrechts, J., Nusbaum, M.P., Bosch, L. Vanden, Baggerman, G., De Loof, A., Schoofs, L., 2003. Neuropeptidomic analysis of the brain and thoracic ganglion from the Jonah crab, *Cancer borealis*. Biochem. Biophys. Res. Commun. 308, 535–544. https://doi.org/10.1016/S0006-291X(03)01426-8

Jékely, G., Melzer, S., Beets, I., Kadow, I.C.G., Koene, J., Haddad, S., Holden-Dye, L., 2018. The long and the short of it -A perspective on peptidergic regulation of circuits and behaviour. J. Exp. Biol. 221. https://doi.org/10.1242/jeb.166710

Kahsai, L., Kapan, N., Dircksen, H., Winther, Å.M.E., Nässel, D.R., 2010. Metabolic stress responses in *Drosophila* are modulated by brain neurosecretory cells that produce multiple neuropeptides. PLoS One 5, e11480. https://doi.org/10.1371/journal.pone.0011480

Kalra, S.P., Sahu, A., Dube, M.G., Kalra, P.S., 1991. Effects of various tachykinins on pituitary LH secretion, feeding, and sexual behavior in the rat. Ann. N. Y. Acad. Sci. 632, 332–338. https://doi.org/10.1111/j.1749-6632.1991.tb33120.x

Katz, P., Calin-Jageman, R., 2008. Neuromodulation, in: Encyclopedia of Neuroscience. pp. 497–503.

Katz, P.S., Frost, W.N., 1996. Intrinsic neuromodulation: altering neuronal circuits from within. Trends Neurosci. 19, 54–61.

Khornchatri, K., Kornthong, N., Saetan, J., Tinikul, Y., Chotwiwatthanakun, C., Cummins, S.F., Hanna, P.J., Sobhon, P., 2015. Distribution of serotonin and dopamine in the central nervous system of the female mud crab, *Scylla olivacea* (Herbst). Acta Histochem. 117, 196–204. https://doi.org/10.1016/j.acthis.2014.12.006

Kim, S.M., Su, C.-Y., Wang, J.W., 2017. Neuromodulation of innate behaviors in *Drosophila*. Annu. Rev. Neurosci. 40, 327–348. https://doi.org/10.1146/annurev-neuro-072116-031558

Kononenko, N.L., Hartfil, S., Willer, J., Ferch, J., Wolfenberg, H., Pfluger, H-J., 2018. A population of descending tyraminergic/octopaminergic projection neurons of the insect deutocerebrum. J Comp Neurol. 527, 1027-2038.

Kornthong, N., Tinikul, Y., Khornchatri, K., Saeton, J., Magerd, S., Suwansa-Ard, S., Kruangkum, T., Hanna, P.J., Sobhon, P., 2014. Neuronal classification and distribution in the central nervous system of the female mud crab, *Scylla olivacea*. Microsc. Res. Tech. 77, 189–200. https://doi.org/10.1002/jemt.22327

Landgraf, R., Neumann, I.D., 2004. Vasopressin and oxytocin release within the brain: a dynamic concept of multiple and variable modes of neuropeptide communication. Front. Neuroendocrinol. 25, 150–176. https://doi.org/10.1016/j.yfrne.2004.05.001

Li, L., Kelley, W.P., Billimoria, C.P., Christie, A.E., Pulver, S.R., Sweedler, J. V., Marder, E., 2003. Mass spectrometric investigation of the neuropeptide complement and release in the pericardial organs of the crab, *Cancer borealis*. J. Neurochem. 87, 642–656. https://doi.org/10.1046/j.1471-4159.2003.02031.x

Lin, X., Volkoff, H., Narnaware, Y., Bernier, N.J., Peyon, P., Peter, R.E., 2000. Brain regulation of feeding behavior and food intake in fish. Comp. Biochem. Physiol. - A Mol. Integr. Physiol. 126, 415–434. https://doi.org/10.1016/S1095-6433(00)00230-0

Mangerich, S., Keller, R., 1988. Localization of pigment-dispersing hormone (PDH) immunoreactivity in the central nervous system of *Carcinus maenas* and *Orconectes limosus* (Crustacea), with reference to FMRFamide immunoreactivity in *O. limosus*. Cell Tissue Res. 253, 199–208. https://doi.org/10.1007/BF00221755

Marder, E., Bucher, D., 2007. Understanding circuit dynamics using the stomatogastric nervous system of lobsters and crabs. Annu. Rev. Physiol. 69, 291–316. https://doi.org/10.1146/annurev.physiol.69.031905.161516

Matsumoto, K., 1954. Neurosecretion in the thoracic ganglion of the crab, *Eriocheir japonicus*. Biol. Bull. 106, 60–68. https://doi.org/10.2307/1538779

Maynard, D.M., 1961. Thoracic neurosecretory structures in brachyura. II. Secretory neurons. Gen. Comp. Endocrinol. 1, 237–263. https://doi.org/10.1016/0016-6480(61)90033-8

McDonald, J.H., 2014. Handbook of biological statistics (3rd ed.). Sparky House Publishing, Baltimore, Maryland.

McGaw, I.J., 2005. The decapod crustacean circulatory system: A case that is neither open nor closed. Microsc. Microanal. 11, 18–36. https://doi.org/10.1017/S1431927605050026

McGaw, I.J., Reiber, C.L., 2002. Cardiovascular system of the blue crab *Callinectes sapidus*. J. Morphol. 251, 1–21. https://doi.org/10.1002/jmor.1071

Messinger, D.I., Kutz, K., Le, T., Verley, D.R., Hsu, Y-W.A., Ngo, C.T., Cain, S.D., Birmingham, J.T., Li, L., Christie, A.E., 2005. Identification and characterization of a tachykinin-containing neuroendocrine organ in the commissural ganglion of the crab *Cancer productus*. J. Exp. Biol. 208, 3303–3319. https://doi.org/10.1242/jeb.01787

Nässel, D.R., 1984. Ultrastructural demonstration of serotonin-immunoreactivity in the nervous system of an insect (*Calliphora erythrocephala*). Neurosci Lett 48, 203–210.

Nässel, D.R., 1999. Tachykinin-related peptides in invertebrates: a review. Peptides 20, 141–58.

Nässel, D.R., 2006. Tachykinins and tachykinin-related peptides in invertebrates. Handb. Biol. Act. Pept. 20, 171–176. https://doi.org/10.1016/B978-012369442-3/50029-5

Nässel, D.R., Homberg, U., 2006. Neuropeptides in interneurons of the insect brain. Cell Tissue Res. https://doi.org/10.1007/s00441-006-0210-8

Nässel, D.R., Zandawala, M., Kawada, T., Satake, H., 2019. Tachykinins: Neuropeptides that are ancient, diverse, widespread and functionally pleiotropic. Front. Neurosci. 13, 1–26. https://doi.org/10.3389/fnins.2019.01262

Nusbaum, M.P., Blitz, D.M., 2012. Neuropeptide modulation of microcircuits. Curr. Opin. Neurobiol. https://doi.org/10.1016/j.conb.2012.01.003

Nusbaum, M.P., Blitz, D.M., Marder, E., 2017. Functional consequences of neuropeptide and small-molecule co-transmission. Nat. Rev. Neurosci. 18, 389–403. https://doi.org/10.1038/nrn.2017.56

Peña, F., Ramirez, J.-M., 2004. Substance P-mediated modulation of pacemaker properties in the mammalian respiratory network. J. Neurosci. 24, 7549–7556. https://doi.org/20026330

Pérez, C.T., Hill, R.H., Grillner, S., 2007. Endogenous tachykinin release contributes to the locomotor activity in lamprey. J. Neurophysiol. 97, 3331–3339. https://doi.org/10.1152/jn.01302.2006

Persson, M.G.S., Nässel, D.R., 1999. Neuropeptides in insect sensory neurones: tachykinin-, FMRFamide- and allatotropin-related peptides in terminals of locust thoracic sensory afferent. Brain Res. 816, 131–141.

Piehp, F., Arvidsson, U., Hiikfelt, T., Cullheim, S., 1993. Calcitonin gene-related peptide-like immunoreactivity in motoneuron pools innervating different hind limb muscles in the rat. Exp Brain Res 96, 291–303.

Pilkington, J.B., MacFarlane, D.W., 1978. Numbers and central projections of crab second maxilla motor neurones. J. Mar. Biol. Assoc. United Kingdom 58, 571–584. https://doi.org/10.1017/S0025315400041230

Richardson, D.S., Lichtman, J.W., 2015. Clarifying tissue clearing. Cell 162, 246–257. https://doi.org/10.1016/j.cell.2015.06.067

Robertson, R.M., Laverack, M.S., 1979. The structure and function of the labrum in the lobster *Homarus gammarus* (L.). Proc. R. Soc. Lond. B. Biol. Sci. 206, 209–233. https://doi.org/10.1098/rspb.1979.0102

Rosenfeld, M.G., Mermod, J.J., Amara, S.G., Swanson, L.W., Sawchenko, P.E., Rivier, J., Vale, W.W., Evans, R.M., 1983. Production of a novel neuropeptide encoded by the calcitonin gene via tissue-specific RNA processing. Nature 304, 129–135. https://doi.org/10.1038/304129a0

Saetan, J., Senarai, T., Tamtin, M., Weerachatyanukul, W., Chavadej, J., Hanna, P.J., Parhar, I., Sobhon, P., Sretarugsa, P., 2013. Histological organization of the central nervous system and distribution of a gonadotropin-releasing hormone-like peptide in the blue crab, *Portunus pelagicus*. Cell Tissue Res. 353, 493–510. https://doi.org/10.1007/s00441-013-1650-6

Sandeman, D., Atwood, H., 1982. Crustacean central nervous system: Neuron projections in the ventral ganglia, in: The Biology of Crustacea, Neurobiology, Structure and Function. Academic Press, pp. 40–56.

Sandeman, R.E., Sandeman, D.C., Watson, A.H.D., 1990. Substance P antibody reveals homologous neurons with axon terminals among somata in the crayfish and crab brain. J. Comp. Neurol. 294, 569–582. https://doi.org/10.1002/cne.902940405

Schmidt, M., 1997. Distribution of presumptive chemosensory afferents with FMRFamide- or substance P-like immunoreactivity in decapod crustaceans. Brain Res. 746, 71–84. https://doi.org/10.1016/S0006-8993(96)01187-0

Schmidt, M., Ache, B.W., 1994. Descending neurons with dopamine-like or with substance P/FMRFamide-like immunoreactivity target the somata of olfactory interneurons in the brain of the spiny lobster, *Panulirus argus*. Cell Tissue Res. 278, 337–352. https://doi.org/10.1007/BF00414177

Schneider, H., Trimmer, B.A., Rapus, J., Eckert, M., Valentine, D.E., Kravitz, E.A., 1993. Mapping of octopamine-immunoreactive neurons in the central nervous system of the lobster. J. Comp. Neurol. 329, 129–142. https://doi.org/10.1002/cne.903290109

Senarai, T., Saetan, J., Tamtin, M., Weerachatyanukul, W., Sobhon, P., Sretarugsa, P., 2016. Presence of gonadotropin-releasing hormone-like peptide in the central nervous system and reproductive organs of the male blue swimming crab, *Portunus pelagicus*, and its effect on spermatogenesis. Cell Tissue Res. 365, 265–277.

Seo, J., Choe, M., Kim, S.Y., 2016. Clearing and labeling techniques for large-scale biological tissues. Mol. Cells 39, 439–446. https://doi.org/10.14348/molcells.2016.0088

Silvestri, L., Costantini, I., Sacconi, L., Pavone, FS., 2016. Clearing of fixed tissue: a review from a microscopist's perspective. J Biomed Opt. 21, 081205.

Skiebe, P., 2001. Neuropeptides are ubiquitous chemical mediators: Using the stomatogastric nervous system as a model system. J Exp Biol 204, 2035–48.

Smarandache-Wellman, C.R., 2016. Arthropod neurons and nervous system. Curr. Biol. 26, R960–R965. https://doi.org/10.1016/j.cub.2016.07.063

Smith, S.J., Smbül, U., Graybuck, L.T., Collman, F., Seshamani, S., Gala, R., Gliko, O., Elabbady, L., Miller, J.A., Bakken, T.E., Rossier, J., Yao, Z., Lein, E., Zeng, H., Tasic, B., Hawrylycz, M., 2019. Single-cell transcriptomic evidence for dense intracortical neuropeptide networks. Elife 8, 1–35. https://doi.org/10.7554/eLife.47889

Stein, W., 2009. Modulation of stomatogastric rhythms. J. Comp. Physiol. A Neuroethol. Sensory, Neural, Behav. Physiol. 195, 989–1009. https://doi.org/10.1007/s00359-009-0483-y

Stein, W., DeLong, N.D., Wood, D.E., Nusbaum, M.P., 2007. Divergent co-transmitter actions underlie motor pattern activation by a modulatory projection neuron. Eur. J. Neurosci. 26, 1148–1165. https://doi.org/10.1111/j.1460-9568.2007.05744.x

Steinhoff, M.S., von Mentzer, B., Geppetti, P., Pothoulakis, C., Bunnett, N.W., 2014. Tachykinins and their receptors: Contributions to physiological control and the mechanisms of disease. Physiol. Rev. 94, 265–301. https://doi.org/10.1152/physrev.00031.2013

Stephens, P.J., 1986. The fused thoracic-abdominal ganglion of the hermit crab (*Pagurus pollicaris*): Neuromuscular relationships in the thoracic and abdominal flexor muscles. J. Exp. Biol. 123, 201–216.

Stewart, M.J., Stewart, P., Sroyraya, M., Soonklang, N., Cummins, S.F., Hanna, P.J., Duan, W., Sobhon, P., 2013. Cloning of the crustacean hyperglycemic hormone and evidence for molt-inhibiting hormone within the central nervous system of the blue crab *Portunus pelagicus*. Comp. Biochem. Physiol. - A Mol. Integr. Physiol. 164, 276–290. https://doi.org/10.1016/j.cbpa.2012.10.029

Svensson, E., Apergis-Schoute, J., Burnstock, G., Nusbaum, M.P., Parker, D., Schiöth, H.B., 2019. General principles of neuronal co-transmission: Insights from multiple model systems. Front. Neural Circuits. https://doi.org/10.3389/fncir.2018.00117

Swallie, S.E., Monti, A.M., Blitz, D.M., 2015. Anatomical organization of multiple modulatory inputs in a rhythmic motor system. PLoS One 10. https://doi.org/10.1371/journal.pone.0142956

Swensen, A.M., Marder, E., 2000. Multiple peptides converge to activate the same voltage-dependent current in a central pattern-generating circuit. J Neurosci 20, 6752–6759.

Taghert, P.H., Nitabach, M.N., 2012. Peptide neuromodulation in invertebrate model systems. Neuron 76, 82–97. https://doi.org/10.1016/j.neuron.2012.08.035

Thorn, K., Chamberlain, C., Tang, N., 2007. Optimal clearing and mounting media for confocal microscopy of thick specimens, Web Article. Nikon Imaging Centre at University of California. https://doi.org/10.1017/CBO9781107415324.004

Vigouroux, R.J., Belle, M., Chédotal, A., 2017. Neuroscience in the third dimension: Shedding new light on the brain with tissue clearing. Mol. Brain 10. https://doi.org/10.1186/s13041-017-0314-y

Vilim, F.S., Cropper, E.C., Price, D.A., Kupfermann, I., Weiss, K.R., 2000. Peptide cotransmitter release from motorneuron B16 in *Aplysia californica*: Costorage, corelease, and functional implications. J. Neurosci. 20, 2036–2042. https://doi.org/10.1523/jneurosci.20-05-02036.2000

Walder, K.K., Ryan, S.B., Bzdega, T., Olszewski, R.T., Neale, J.H., Lindgren, C.A., 2013. Immunohistological and electrophysiological evidence that N-acetylaspartylglutamate is a co-transmitter at the vertebrate neuromuscular junction. Eur. J. Neurosci. 37, 118–129. https://doi.org/10.1111/ejn.12027

Wales, W., Macmillan, D.L., Laverack, M.S., 1976. Mandibular movements and their control in *Homarus gammarus* - II. The normal cycle. J. Comp. Physiol. A 106, 193–206. https://doi.org/10.1007/BF00620498

Whim, M.D., Church, P.J., Lloyd, P.E., 1993. Functional roles of peptide cotransmitters at neuromuscular synapses in *Aplysia*. Mol. Neurobiol. 7, 335–347. https://doi.org/10.1007/BF02769181

White, R.S., Nusbaum, M.P., 2011. The same core rhythm generator underlies different rhythmic motor patterns. J. Neurosci. 31, 11484–11494. https://doi.org/10.1523/JNEUROSCI.1885-11.2011

Winther, A.M.E., Acebes, A., Ferrús, A., 2006. Tachykinin-related peptides modulate odor perception and locomotor activity in *Drosophila*. Mol. Cell. Neurosci. 31, 399–406. https://doi.org/10.1016/j.mcn.2005.10.010

Wood, D.E., Derby, C.D., 1996. Distribution of dopamine-like immunoreactivity suggests a role for dopamine in the courtship display behavior of the blue crab, *Callinectes sapidus*. Cell Tissue Res. 285, 321–330. https://doi.org/10.1007/s004410050649

Wood, D.E., Stein, W., Nusbaum, M.P., 2000. Projection neurons with shared cotransmitters elicit different motor patterns from the same neural circuit. J Neurosci 20, 8943.

Yasuda-Kamatani, Y., Yasuda, A., 2006. Characteristic expression patterns of allatostatin-like peptide, FMRFamide-related peptide, orcokinin, tachykinin-related peptide, and SIFamide in the olfactory system of crayfish *Procambarus clarkii*. J. Comp. Neurol. 496, 135–147. https://doi.org/10.1002/cne.20903

Yasuda, A., Yasuda-Kamatani, Y., Nozaki, M., Nakajima, T., 2004. Identification of GYRKPPFNGSIFamide (crustacean-SIFamide) in the crayfish *Procambarus clarkii* by topological mass spectrometry analysis. Gen. Comp. Endocrinol. 135, 391–400. https://doi.org/10.1016/j.ygcen.2003.10.001

Yu,Q., OuYang, C., Liang, Z., Li, L., 2014. Mass spectrometric characterization of the crustacean neuropeptidome. EuPA Open Proteomics 3, 152-170.

Zucker, R.M., Hunter III, E.S., Rogers, J.M., 2000. Confocal laser scanning microscopy of morphology and apoptosis in organogenesis-stage mouse embryos, in: Walker, J.M., Tuan, R.S., Lo, C.W. (Eds.), Methods in Molecular Biology. Humana Press, Totowa, NJ, pp. 191–202. https://doi.org/10.1007/978-1-4939-9182-2_20

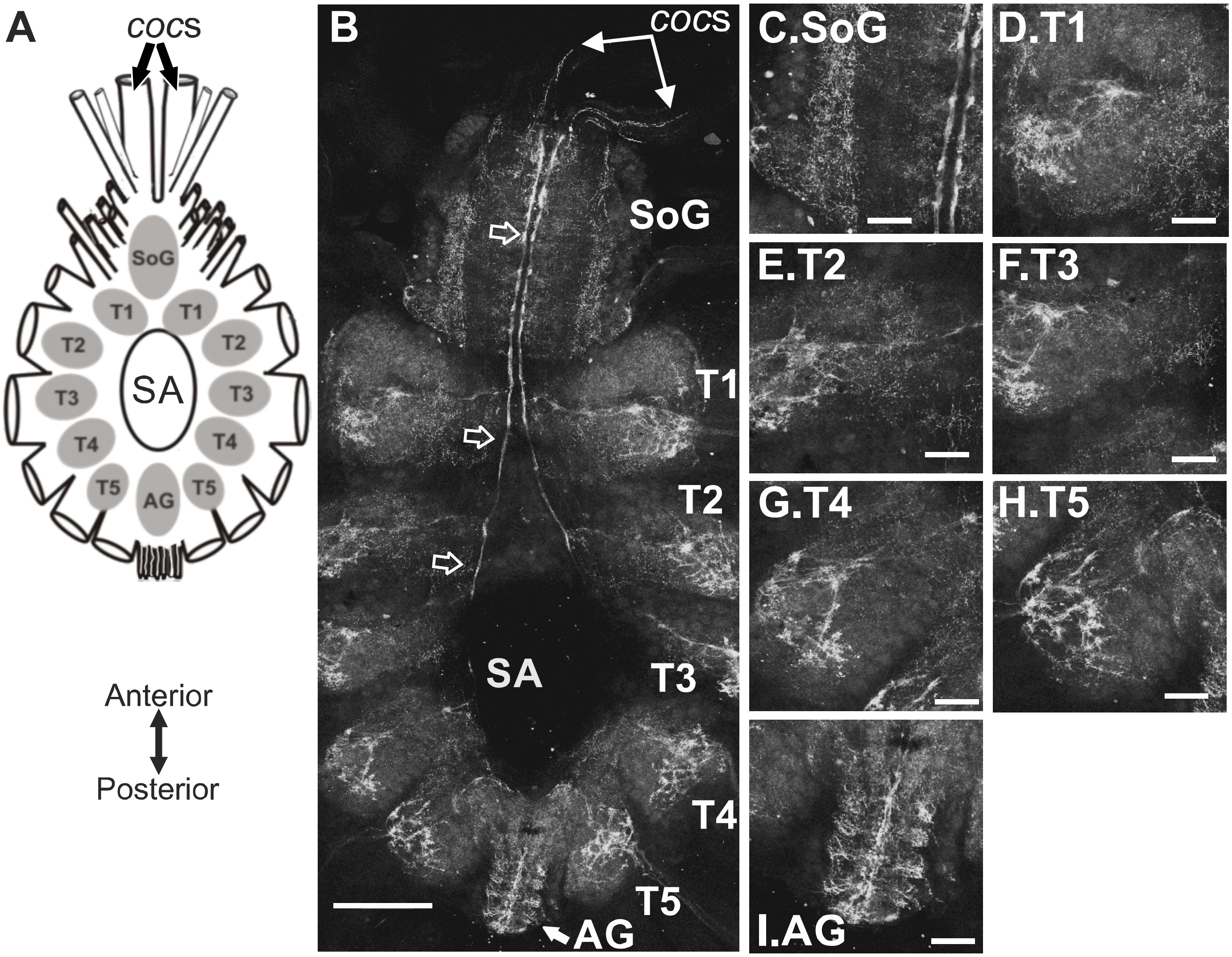
A
cocs
SoG
T1
T1
T2
T2
SA
T3
T3
T4
T4
T5
AG
T5
Anterior
Posterior
B
cocs
SoG
T1
T2
SA
T3
T4
T5
AG
C.SoG
D.T1
E.T2
F.T3
G.T4
H.T5
I.AG

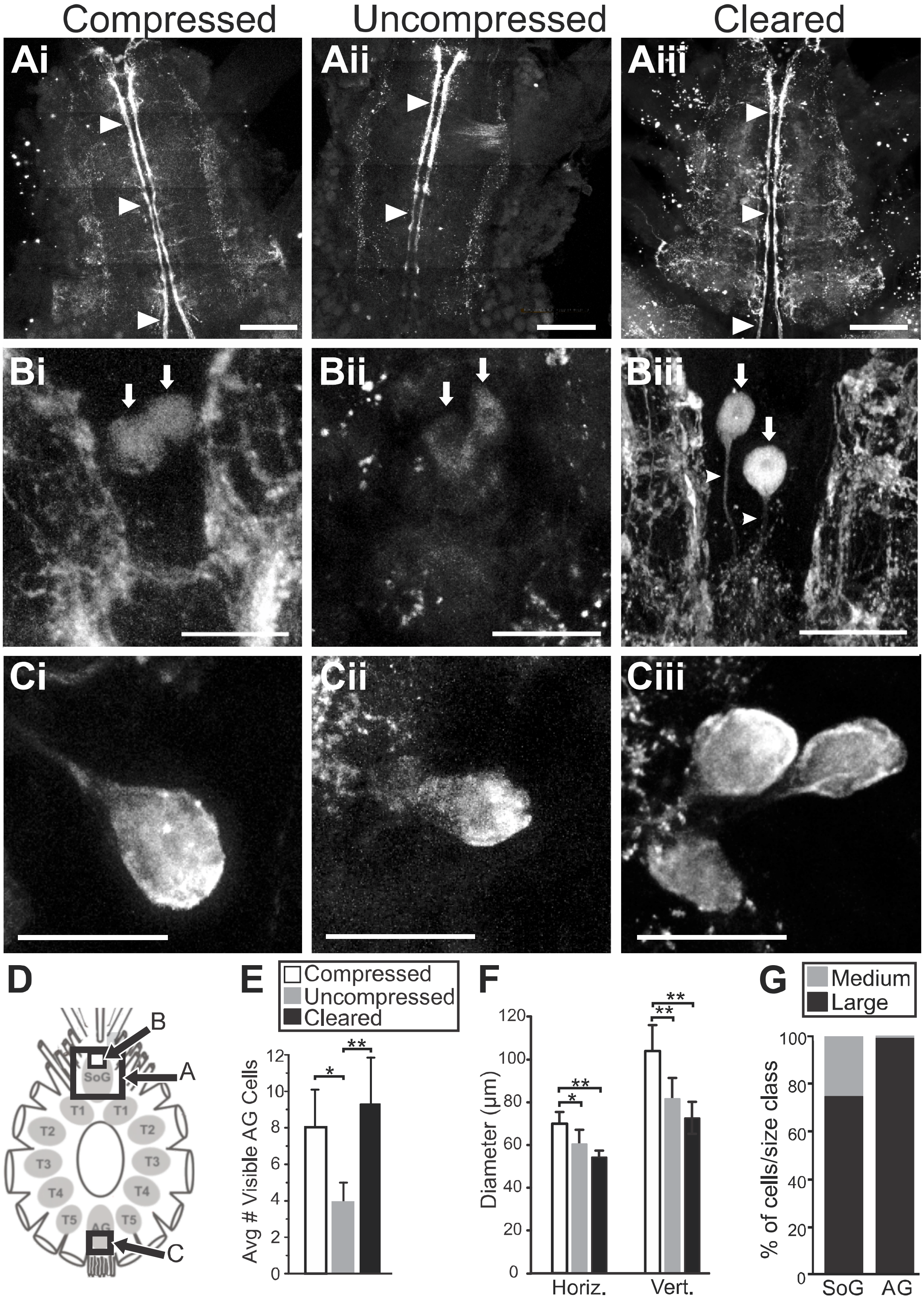
Compressed
Uncompressed
Cleared
Ai
Aii
Aiii
Bi
Bii
Biii
Ci
Cii
Ciii
D
B
A
SoG
T1
T1
T2
T2
T3
T3
T4
T4
T5
AG
T5
C
E
Compressed
Uncompressed
Cleared
Avg # Visible AG Cells
0
2
4
6
8
10
12
*
**
F
Diameter (µm)
0
20
40
60
80
100
120
*
**
**
**
Horiz.
Vert.
G
Medium
Large
% of cells/size class
0
20
40
60
80
100
SoG
AG

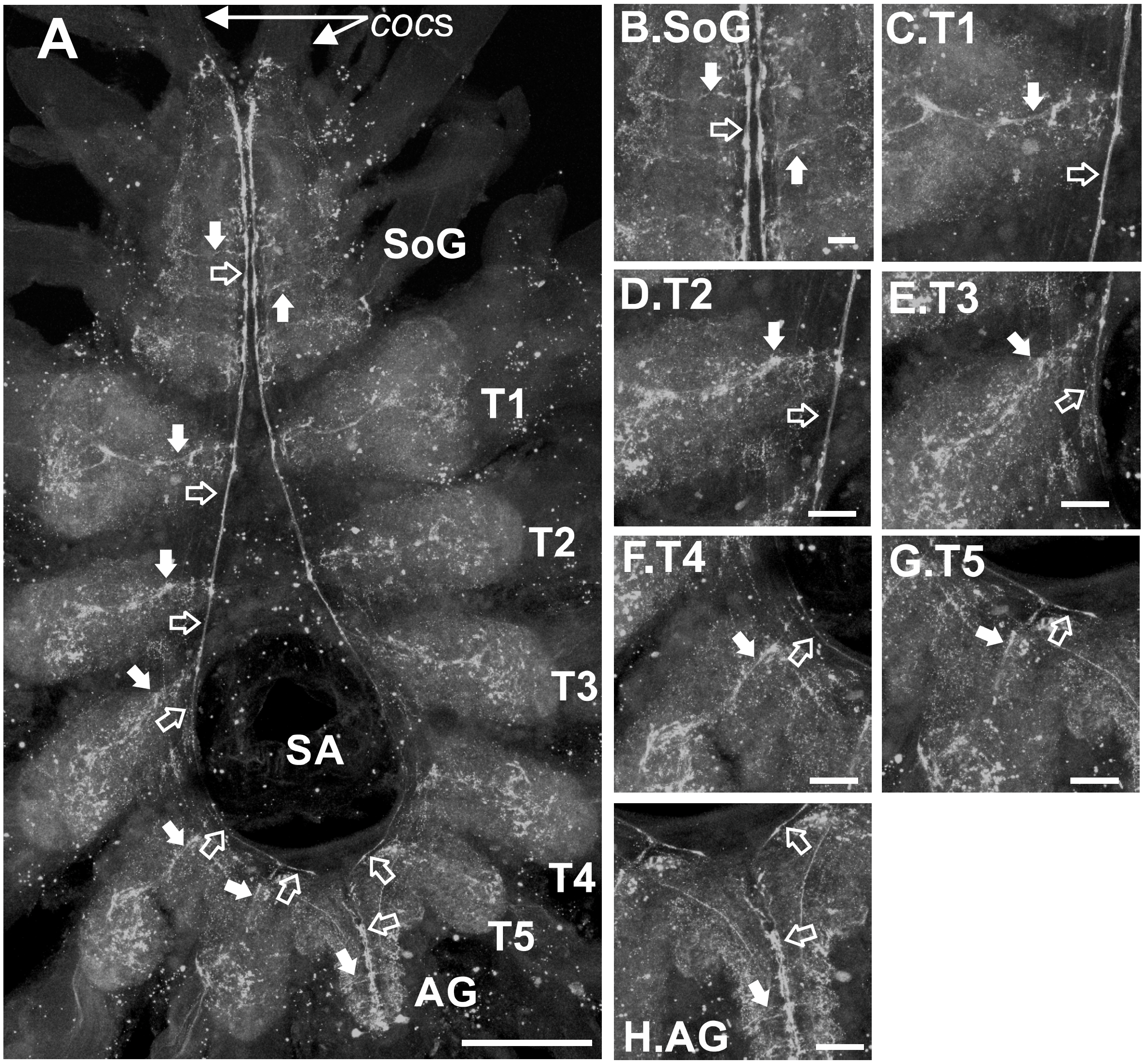
A
COCS
SoG
T1
T2
T3
SA
T4
T5
AG
B.SoG
C.T1
D.T2
E.T3
F.T4
G.T5
H.AG

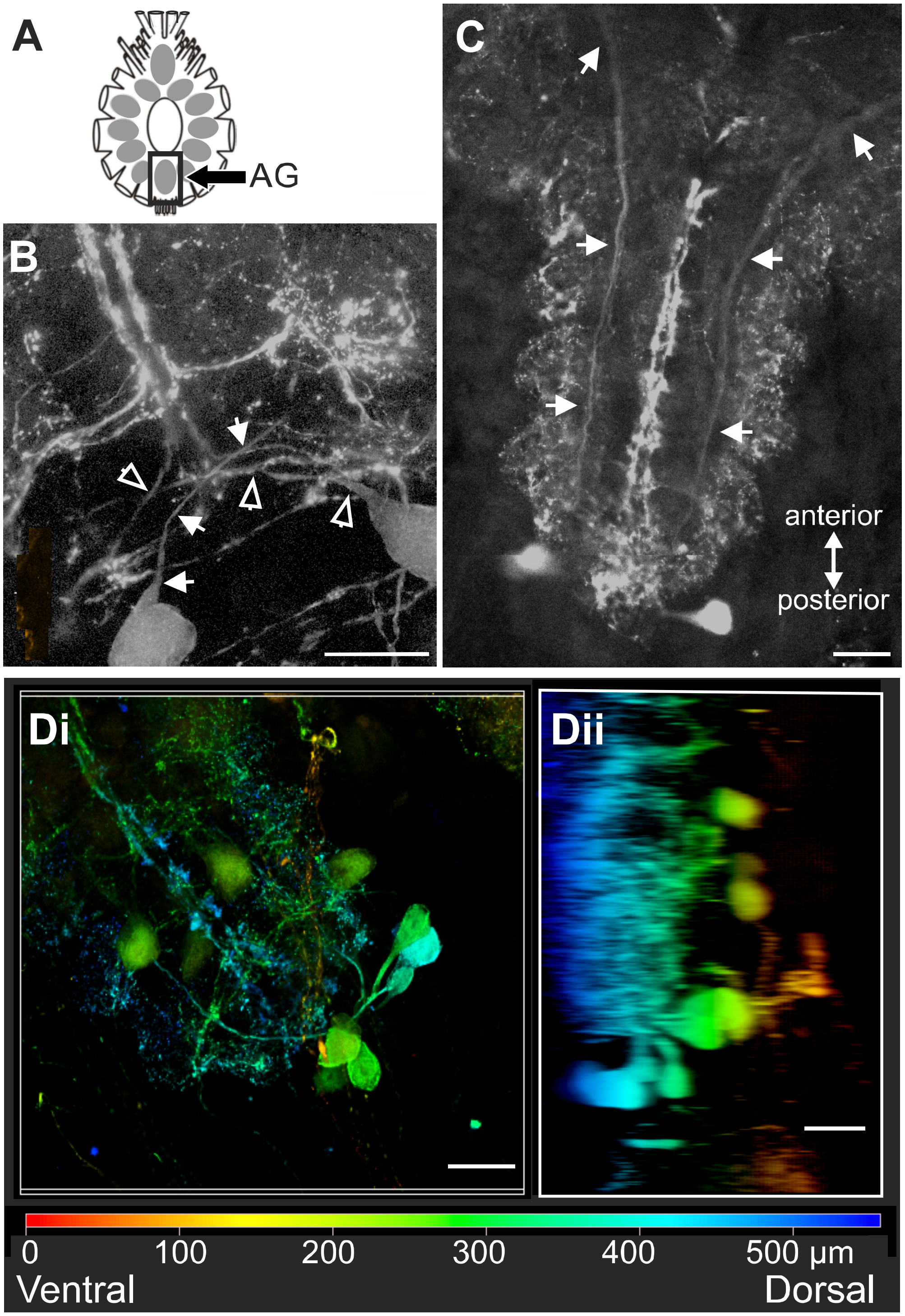
A
AG
B
C
anterior
posterior
Di
Dii
0
100
200
300
400
500 μm
Ventral
Dorsal

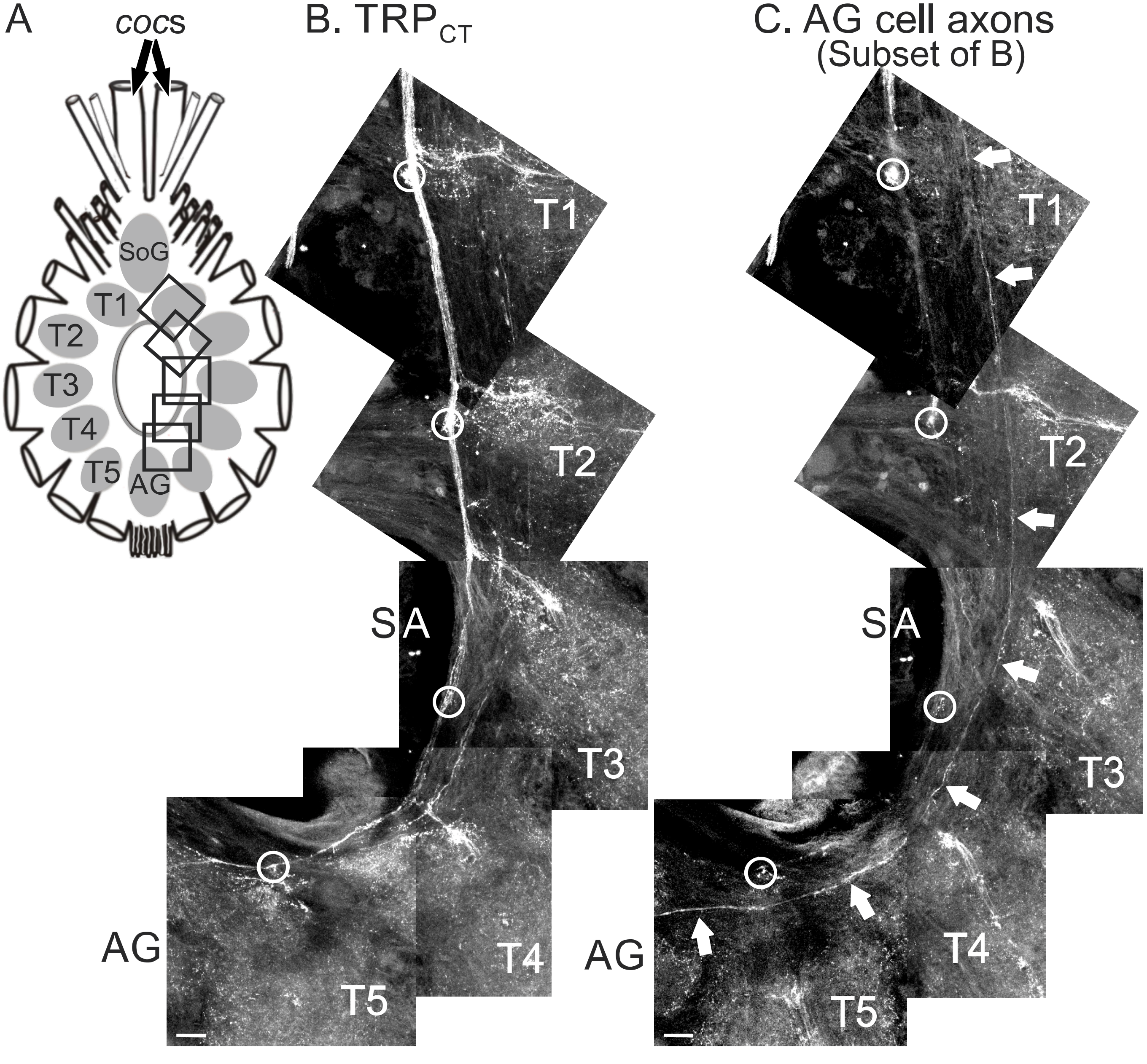
A

B. TRP_{CT}

C. AG cell axons (Subset of B)

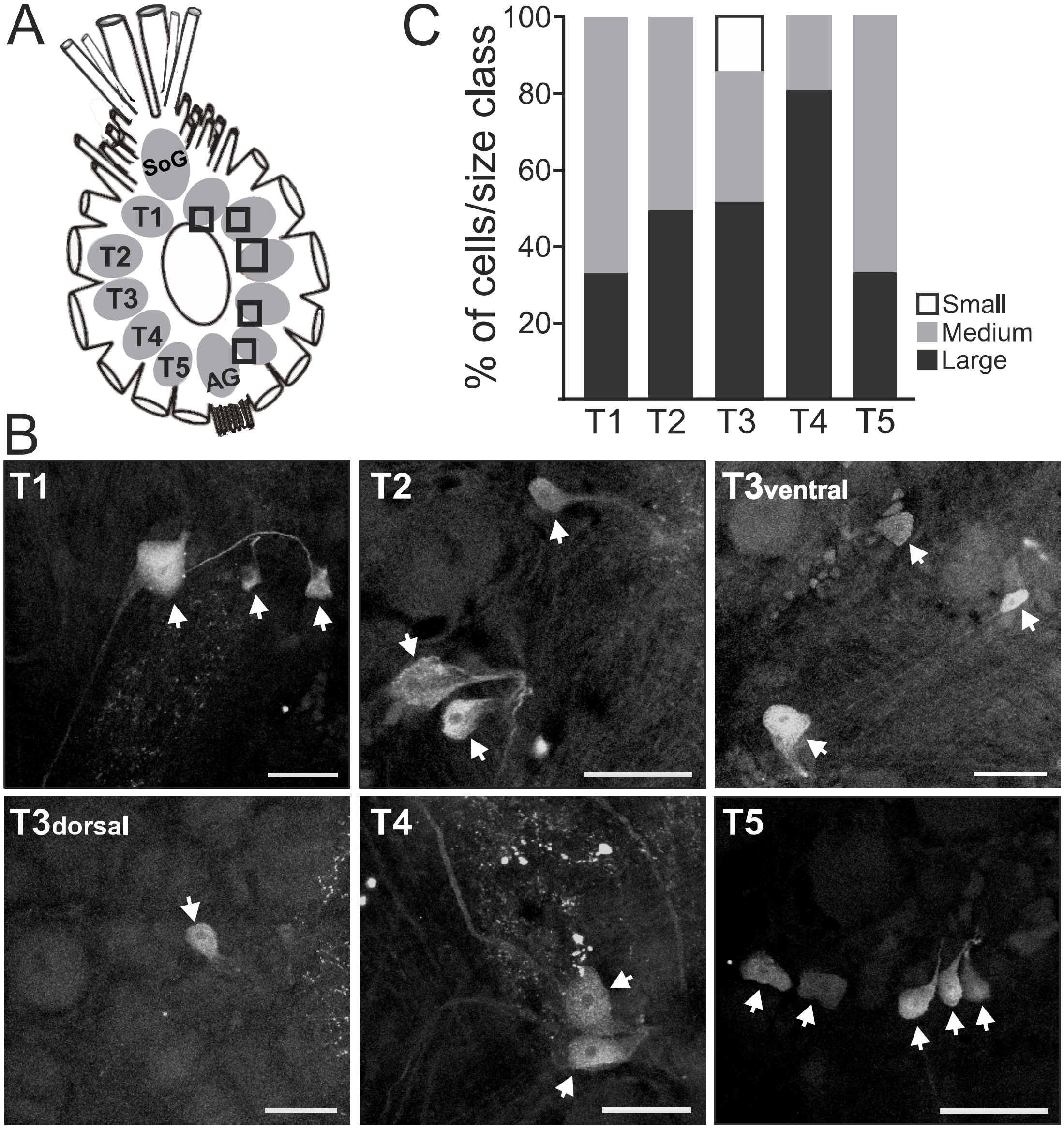
A
SoG
T1
T2
T3
T4
T5
AG
C
% of cells/size class
100
80
60
40
20
T1
T2
T3
T4
T5
Small
Medium
Large
B
T1
T2
T3ventral
T3dorsal
T4
T5

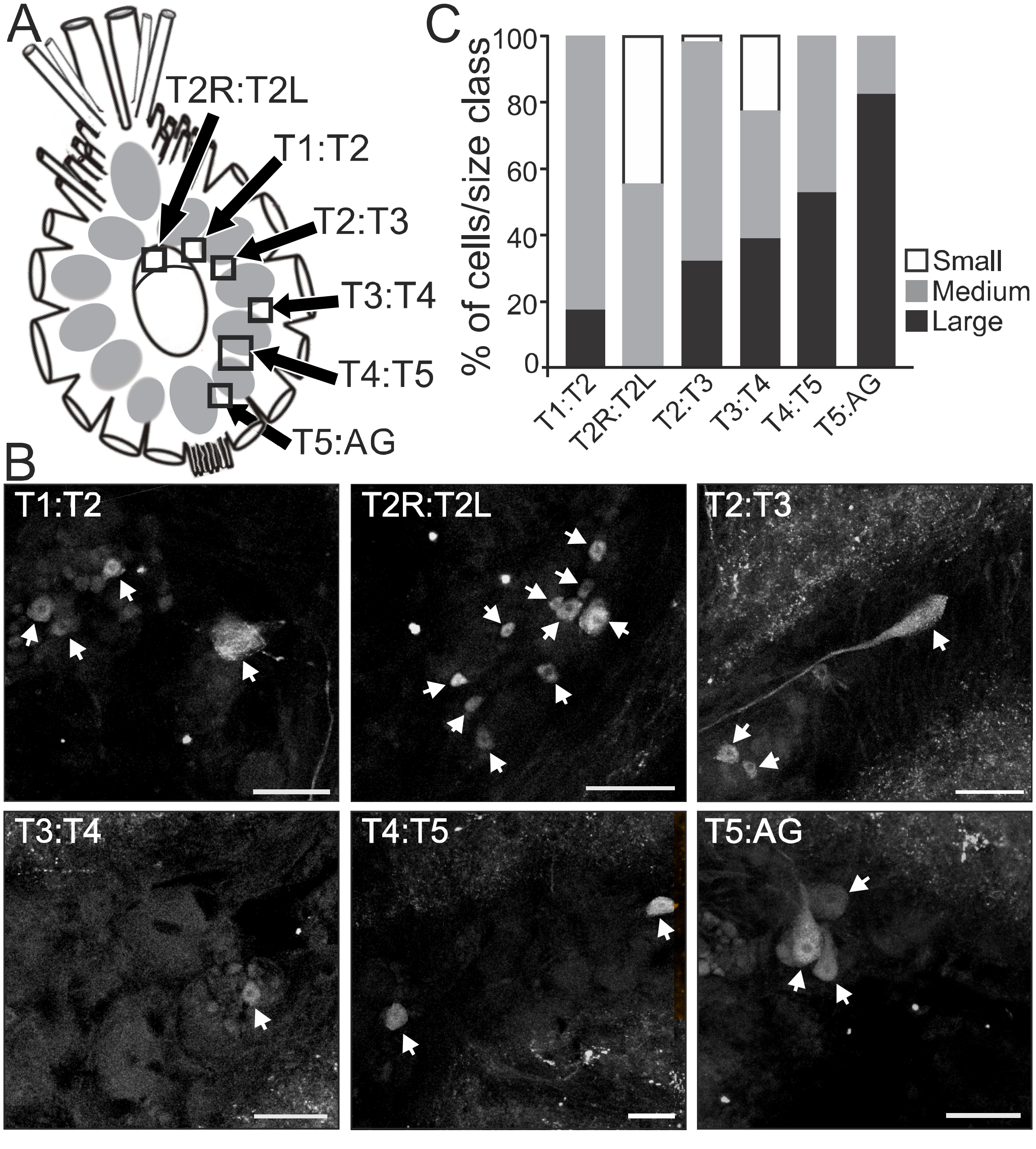
A
T2R:T2L
T1:T2
T2:T3
T3:T4
T4:T5
T5:AG
C
% of cells/size class
100
80
60
40
20
0
Small
Medium
Large
T1:T2
T2R:T2L
T2:T3
T3:T4
T4:T5
T5:AG
B
T1:T2
T2R:T2L
T2:T3
T3:T4
T4:T5
T5:AG